ONLINE METHODS

Mouse, common marmoset and human PSCs. Mouse ESCs were obtained from Laboratory of Pluripotent Cell Studies, RIKEN Center for Developmental Biology. Common marmoset ESCs (cmESCs) were obtained from Central Institute for Experimental Animals. The human ESC lines (khESC-1, 2 and 3) were obtained from Department of Development and Differentiation, Institute for Frontier Medical Sciences, Kyoto University and were used in conformity with The Guidelines for Derivation and Utilization of Human Embryonic Stem Cells of the Ministry of Education, Culture, Sports, Science and Technology, Japan. Mouse (iPS-MEF-Ng-20D-17) and human (253G4) iPSCs were obtained from Center for iPSC Research and Application, Kyoto University.

Animals. All animals including pregnant and neonatal Wistar rats, and NOD-SCID mice (10 weeks old, male), were purchased from Japan CLEA.

All experimental procedures and protocols were approved by the Animal Care and Use Committees of the Keio University and conformed to the US National Institutes of Health Guide for the Care and Use of Laboratory Animals.

Reagents. MitoTracker dyes (Deep Red, Red, Orange and Green), TMRM, 5,5′,6,6′-tetrachloro-1,1′,3,3′-tetraethylbenzimidazolylcarbocyanine iodide (JC-1), nonyl acridine orange (NAO) and Rhodamine 123 were purchased from Invitrogen. These mitochondria-selective fluorescent dyes can be divided into the Nernstian or non-Nernstian dye groups. The former, including TMRM, can enter into and exit from the mitochondrial matrix freely depending on the mitochondrial membrane potential. In contrast, non-Nernstian dyes such as the MitoTracker dyes cannot exit freely[21]. This characteristic difference may reflect their toxicities and can be used case by case for research, for example, non-Nernstian dyes are used for long-term staining.

The mouse monoclonal antibody to α-actinin (used at 1:400 dilution) was purchased from Sigma-Aldrich. The goat polyclonal antibody to GATA-4 (C-20) and the goat polyclonal antibody for Nkx2.5 (N-19) were purchased from Santa Cruz biotechnology. The mouse monoclonal antibody for SdhB (1:100), Alexa Fluor 488 donkey anti-mouse IgG antibody and Alexa Fluor 546 donkey anti-goat immunoglobulin gamma (IgG) were purchased from Invitrogen.

Maintenance of mouse, marmoset and human PSCs. We maintained mouse ESCs and iPSCs on gelatin-coated dishes in Glasgow Minimum Essential Medium (Sigma) supplemented with 10% FBS (FBS; Equitechbio), 0.1 mM MEM Non-Essential Amino Acids solution (Sigma), 2 mM L-glutamine (Sigma), 0.1 mM β-mercaptoethanol (Sigma) and 2,000 U ml^{-1} mouse LIF (Chemicon). We maintained cmESCs on mouse embryonic fibroblasts in Knockout Dulbecco's Modified Eagle's Medium (KO-DMEM; Invitrogen) supplemented with 20% Knockout Serum Replacement (KSR; Invitrogen), 0.1 mM MEM Non-Essential Amino Acids solution, 2 mM L-glutamine, 0.1 mM β-mercaptoethanol and 4 ng ml^{-1} basic fibroblast growth factor (bFGF; Wako Pure Chemical). We maintained human ESCs and iPSCs similarly to cmESCs, except that Dulbecco's Modified Eagle's Medium/Nutrient Mixture F-12 Ham 1:1 (DMEM-F12; Sigma) was used instead of KO-DMEM.

Differentiation of mouse PSC–derived cardiomyocytes. We performed *in vitro* differentiation of mouse ESCs and iPSCs as described below. We collected mouse PSCs with 0.25% trypsin-EDTA and dissociated them. Seventy-five cells were formed to one embryoid body in one hanging drop with alpha-modified Eagle medium (αMEM; Sigma) supplemented with 10% FBS (Equitechbio). On day 2, we transferred embryoid bodies into floating culture plate with new medium. Four to five days after differentiation, floating embryoid bodies were transferred into attachment culture with nonserum culture medium: αMEM supplemented with insulin-transferrin-selenium (ITS; Sigma). Typically, beating cells appeared on day 7. Embryoid bodies were used for purification experiments between days 12 and 25.

Differentiation of cmESC–derived cardiomyocytes. We performed differentiation of cmESCs as follows. The colonies were detached with 0.1% type three collagenase (Worthington Biochemical) and cultured in cmESC medium lacking bFGF or αMEM and supplemented with 10% FBS (SAFC Biosciences) and 0.1 mM β-mercaptoethanol in bacterial Petri dishes to form embryoid bodies. Typically, 5–20% of embryoid bodies contained beating cells. Embryoid bodies were washed three times with αMEM between days 18 and 25, and cultured with αMEM supplemented with ITS. Embryoid bodies were used for purification experiments between days 30 and 50.

Differentiation of human PSC–derived cardiomyocytes. We grew the detached undifferentiated colonies of human ESCs and iPSCs with αMEM supplemented with 20% FBS (SAFC Biosciences) and 0.1 mM β-mercaptoethanol in bacterial Petri dishes to form embryoid bodies. We observed embryoid bodies containing rhythmically beating cells 16–20 d later. Typically, 1–5% of embryoid bodies contained beating cells. From days 20 to 40, embryoid bodies were washed three times with αMEM and cultured with αMEM supplemented with ITS. Embryoid bodies were used for purification experiments between days 50 and 90.

Staining of cultured embryos. We isolated E11.5 and E12.5 Wistar rat embryos and stained with 50 nM TMRM for 4 h in DMEM with 20% FBS at 30% O_2, 5% CO_2 and 37 °C. Then, we changed to medium without TMRM and incubated the embryos for 4 h to remove unbound dye. We observed the fluorescence signal using conventional fluorescence laser microscopy (IX70 microscope (Olympus) equipped with a color charge-coupled device (CCD) camera (CS220; Olympus)).

Staining *in vivo* embryos. We carried out abdominal surgery on the pregnant Wistar rat on postcoital day 11 under deep anesthesia. We carried out a shallow injection of 100 μl of 500 nM MitoTracker Red solution into the placental side of the exposed ovaries. The rat was sustained under anesthesia for 6 h. Then, under deep anesthesia, we removed the embryos from the rat and observed them using fluorescence microscopy. About 20% of the embryos were positive for MitoTracker Red.

Cardiomyocyte purification. We dispersed the minced hearts, whole rat embryos, or intact embryoid bodies using 0.1% collagenase (Worthington Biochemical), 0.25% trypsin (Becton Dickinson), 20 μg ml^{-1} DNase I (Sigma) and the appropriate

doi:10.1038/nmeth.1403

concentration of dyes (10 nM TMRM, 50 nM NAO, 1.5 μM JC-1 or 50 nM MitoTrackers) in Ads buffer (116 mM NaCl, 20 mM HEPES, 12.5 mM NaH_2PO_4, 5.6 mM glucose, 5.4 mM KCl and 0.8 mM $MgSO_4$; pH 7.35) with stirring for 30 min. The dispersed cells were collected and residual cell aggregates were digested again with the same digestion medium. We continued this procedure until all cells were completely dissociated. Finally, all dispersed cells were dissociated with Ads buffer and then analyzed on a FACS (FACS Aria; Becton Dickinson) using 515–545 and 556–601 nm bandpass filters to detect green and red, respectively.

In many cases, nonstained cells exhibited autofluorescence, which may be due to the presence of lipopigments and flavins having broad emission spectrum (450–650 nm)[13]. We suspected that this may affect purity of cardiomyocytes. TMRM can be excited by a 488-nm semiconductor laser and has an emission spectrum that coincides with the red bandpass filter (peak at 575 nm and only 10% of peak fluorescence at 545 nm). Thus, to obtain only cells with high TMRM fluorescence and eliminate contaminating autofluorescent cells, we adopted 'pseudo–two-dimensional separation' in which we observed cells both with red and green filters. In other words, cardiomyocytes received 488 excitation, and then selection for low green and high red fluorescence. Pregating for eliminating doublet fractions, in which one droplet contains more than two cells, was performed according to the manufacturer's instructions.

The TMRM-labeled sorted cells were collected into a tube or were seeded into culture dishes with αMEM containing 10% FBS. For sequential estimation of cardiomyocyte purity, we fixed the sorted cells immediately after collection, then stained them with Nkx2.5 antibody and analyzed again on a FACS. For culture, we used a plate equipped with flexiPERM conA (Greiner Bio-One GmbH) following the manufacturer's instructions. The flexiPERM vessel is a reusable culture funnel, which can adhere tightly onto plastic and glass surfaces. One day after sorting, the flexiPERM vessel was detached from the culture plate and the appropriate amount of medium was added to the plate. This system allowed high-density culture of purified cardiomyocytes in the center of the dish, which enabled good microscopic observation of all cells after detachment of the vessel. For all PSCs, seeded cells were cultured for 5–7 d with αMEM containing 10% FBS, which is necessary for the cells to attach, elongate and develop sarcomere structure, and then fixed and immunofluorescence-stained for α-actinin and Nkx2.5. The culture step is not required for achieving high-purity cardiomyocyte isolation because we have more directly estimated cardiomyocyte purity by sequential FACS analysis.

Transplantation. We purified mouse and human ESC–derived cardiomyocytes, distributed them into nonadhesive 96-well plates (Sumitomo Bakelite) and centrifuged them for 5 min at 100*g*. Two weeks later, the aggregates formed were stained with 50 μM of MitoTracker Red for 2 h in the incubator and washed extensively with Ads buffer. After lightly anesthetizing seven-week-old male NOD-SCID mice with diethylether (Wako Pure Chemical), we intubated them under anesthetization with 1.5% forane (isoflurane, 2-chloro-2-(difluoromethoxy)-1,1,1-trifluoro-ethane) and mechanically ventilated with a Harvard respirator. After this, we performed a left thoracotomy at the third intercostal space and exposed the heart. We inserted a small dead-volume syringe equipped with a 30G needle (Becton Dickinson) containing reaggregated purified cardiomyocytes into the apex, proximally advanced 2–3 mm into the myocardium and released the cells into the myocardium. Then we closed the chest and maintained the mice for 8 weeks before performing a histological examination of these mice.

The 3-(4,5-dimethyl-thiazol-2-yl)-2,5-diphenyltetrazolium bromide (MTT) assay. We treated primary neonatal rat cardiomyocytes with various mitochondrial indicators at 50 nM and 100 nM for 24 h. We added MTT (Wako Pure Chemical) at 0.5 mg ml^{-1} and incubated the cardiomyocytes for 3 h. Then, we dissolved the formazan salt that formed in dimethyl sulfoxide. The absorbance was measured at a wavelength of 550 nm with the background subtracted at 690 nm (SmartSpec3000; Bio-Rad Laboratories). Data were presented as percentage of formazan formation compared to control cells.

Immunofluorescence staining. We fixed cells with 4% paraformaldehyde in phosphate-buffered saline (PBS; pH 7.0) for 20 min. Subsequently, cells were permeabilized with 0.2% Triton X-100 (Sigma) at room temperature (20–28 °C) for 10 min, and then incubated with the primary antibody at 4 °C overnight. Cells were washed with TBS containing 0.1% Tween-20 four times before incubation with the secondary antibodies at room temperature for 30 min. After nuclear staining with DAPI or ToPro-3 (Invitrogen), fluorescence signals were observed using fluorescence microscopy (IX71; Olympus) or confocal laser microscopy (LSM510 META; Carl Zeiss), respectively.

For tissue samples, mice were killed using pentobarbital. The hearts were then perfused from the apex with PBS and fixed by perfusion with 4% paraformaldehyde in PBS (Muto Pure Chemicals). The hearts were then dissected, cryoprotected in sucrose at 4 °C overnight, embedded in OCT compound (Sakura Finetec) and snap-frozen in liquid nitrogen.

Re-aggregation of purified human ESC–derived cardiomyocytes and long-term culture without serum. Human ESC–derived cardiomyocytes were purified and suspended in αMEM supplemented with insulin, transferrin and selenium (ITS) and 0.05% BSA (Invitrogen) in the absence or presence of one of the following growth factors: 25 ng ml^{-1} bFGF (Wako Pure Chemicals); 25 ng ml^{-1} acidic FGF (aFGF); 25 ng ml^{-1} FGF-4; 20 ng ml^{-1} keratinocyte growth factor (KGF); 100 ng ml^{-1} stem cell factor (SCF); 100 ng ml^{-1} vascular endothelial growth factor (VEGF); 10 ng ml^{-1} LIF (Chemicon); 100 ng ml^{-1} glial cell line–derived neurotrophic factor (GDNF); 20 ng ml^{-1} hepatocyte growth factor (HGF); 10 ng ml^{-1} insulin-like growth factor (IGF)-1; 100 ng ml^{-1} epidermal growth factor (EGF); 1×10^{7} M endothelin-1 (ET-1); 10 ng ml^{-1} platelet-derived growth factor (PDGF)-AA; and 100 ng ml^{-1} PDGF-BB. Unless indicated otherwise, growth factors were purchased from R&D Systems Inc. Five hundred cells were distributed into each well ($n = 8$) of cell nonadhesive 96-well plates (MS-0096S; Sumitomo Bakelite) and centrifuged for 5 min at 100*g*.

Total RNA extraction, cDNA synthesis and real-time PCR. Total RNA was prepared from tissues and embryoid bodies using ISOGEN (Nippon gene), according to the manufacturer's instructions. Contaminating genomic DNA was degraded by RNase-free DNase I

doi:10.1038/nmeth.1403

(Ambion) at 37 °C for 30 min. After treatment, DNase I was inactivated by phenol-chloroform extraction and ethanol precipitation. Human heart–derived total RNA was purchased from Takara Bio. We reverse transcribed total RNAs into cDNA using the oligo-(dT)12-18 primer (Superscript II RT kit; Invitrogen). We analyzed the mRNA expression on an ABI 7700 (Applied Biosystems). We listed the target gene name and identification numbers of the primer and probe mixtures (Applied Biosystems) in **Supplementary Table 1**.

21. Jakobs, S. High resolution imaging of live mitochondria. *Biochim. Biophys. Acta.* **1763**, 561–575 (2006).

doi:10.1038/nmeth.1403

Cardiac fibroblasts are essential for the adaptive response of the murine heart to pressure overload

Norifumi Takeda,[1] Ichiro Manabe,[1,2,3] Yuichi Uchino,[1] Kosei Eguchi,[1] Sahohime Matsumoto,[1] Satoshi Nishimura,[1,3] Takayuki Shindo,[3,4] Motoaki Sano,[3,5] Kinya Otsu,[6] Paige Snider,[7] Simon J. Conway,[7] and Ryozo Nagai[1,2,8,9]

[1]Department of Cardiovascular Medicine and [2]Global COE Program, Graduate School of Medicine, University of Tokyo, Tokyo, Japan. [3]PRESTO, Japan Science and Technology Agency, Saitama, Japan. [4]Department of Organ Regeneration, Shinshu University Graduate School of Medicine, Nagano, Japan. [5]Department of Regenerative Medicine and Advanced Cardiac Therapeutics, Keio University School of Medicine, Tokyo, Japan. [6]Department of Cardiovascular Medicine, Osaka University Graduate School of Medicine, Suita, Japan. [7]Riley Heart Research Center, Herman B Wells Center for Pediatric Research, Indiana University of Medicine, Indianapolis, Indiana, USA. [8]Comprehensive Center of Education and Research for Chemical Biology of the Diseases, Graduate School of Medicine, University of Tokyo, Tokyo, Japan. [9]Translational Research Center, University of Tokyo Hospital, Tokyo, Japan.

Fibroblasts, which are the most numerous cell type in the heart, interact with cardiomyocytes in vitro and affect their function; however, they are considered to play a secondary role in cardiac hypertrophy and failure. Here we have shown that cardiac fibroblasts are essential for the protective and hypertrophic myocardial responses to pressure overload in vivo in mice. Haploinsufficiency of the transcription factor–encoding gene Krüppel-like factor 5 (*Klf5*) suppressed cardiac fibrosis and hypertrophy elicited by moderate-intensity pressure overload, whereas cardiomyocyte-specific *Klf5* deletion did not alter the hypertrophic responses. By contrast, cardiac fibroblast–specific *Klf5* deletion ameliorated cardiac hypertrophy and fibrosis, indicating that KLF5 in fibroblasts is important for the response to pressure overload and that cardiac fibroblasts are required for cardiomyocyte hypertrophy. High-intensity pressure overload caused severe heart failure and early death in mice with *Klf5*-null fibroblasts. KLF5 transactivated *Igf1* in cardiac fibroblasts, and IGF-1 subsequently acted in a paracrine fashion to induce hypertrophic responses in cardiomyocytes. *Igf1* induction was essential for cardioprotective responses, as administration of a peptide inhibitor of IGF-1 severely exacerbated heart failure induced by high-intensity pressure overload. Thus, cardiac fibroblasts play a pivotal role in the myocardial adaptive response to pressure overload, and this role is partly controlled by KLF5. Modulation of cardiac fibroblast function may provide a novel strategy for treating heart failure, with KLF5 serving as an attractive target.

Introduction

Myocardial hypertrophy is an essential adaptive process through which the heart responds to various mechanophysical, metabolic, and genetic stresses. However, the hypertrophy induced by sustained overload eventually leads to contractile dysfunction and heart failure through mechanisms that remain poorly understood (1). In addition to enlargement of individual cardiomyocytes, the hypertrophied myocardium exhibits complex structural remodeling that involves rearrangement of the muscle fibers, interstitial fibrosis, accumulation of extracellular matrix, and angiogenesis (2, 3), which implies that the non-muscle cells residing in the interstitium likely play important roles in both cardiac hypertrophy and heart failure. In fact, cells other than cardiomyocytes account for approximately 70% of the total cell number in the heart, with the majority being fibroblasts (4, 5). In addition to extracellular matrix proteins (e.g., collagens), cardiac fibroblasts produce a variety of growth factors that likely mediate an interplay between cardiac fibroblasts and cardiomyocytes. For instance, several humoral factors secreted by cardiac fibroblasts, including cardiotrophin-1 (6), endothelin-1 (7), IL-6 (8), periostin (POSTN) (9), and leukemia inhibitory factor (10), have been shown to induce hypertrophic responses in cultured cardiomyocytes. Cardiac fibroblasts also promote proliferation of cardiomyocytes through paracrine interactions in developing hearts (11). And very recently it was shown that inhibition of a fibroblast-selective miRNA ameliorated cardiac fibrosis, hypertrophy, and dysfunction, suggesting that fibroblasts play a detrimental role in cardiac remodeling (12). Still, the precise function of cardiac fibroblasts during adaptive responses of the myocardium remains unclear (2).

Members of the Krüppel-like factor (KLF) family of transcription factors are important regulators of development, cellular differentiation and growth, and the pathogenesis of various diseases, including cancer and cardiovascular disease (13). We previously used *Klf5*$^{+/-}$ mice to show that KLF5 is required for cardiac hypertrophy and fibrosis in response to continuous infusion of angiotensin II (AII) (14, 15). In primary cultured cardiac fibroblasts, KLF5 directly controls transcription of *Pdgfa*, encoding platelet-derived growth factor A (PDGF-A) (14), which is known to be involved in tissue remodeling and wound healing (16–19). The precise role played by KLF5 in cardiac hypertrophy and heart failure remains unclear, however.

In the present study, we developed conditional *Klf5*-knockout mouse lines to examine the cell type–specific functions of KLF5 in cardiac hypertrophy and heart failure. While cardiomyocyte-specific deletion of *Klf5* did not alter the hypertrophic responses

Conflict of interest: The authors have declared that no conflict of interest exists.
Citation for this article: *J. Clin. Invest.* 120:254–265 (2010). doi:10.1172/JCI40295.

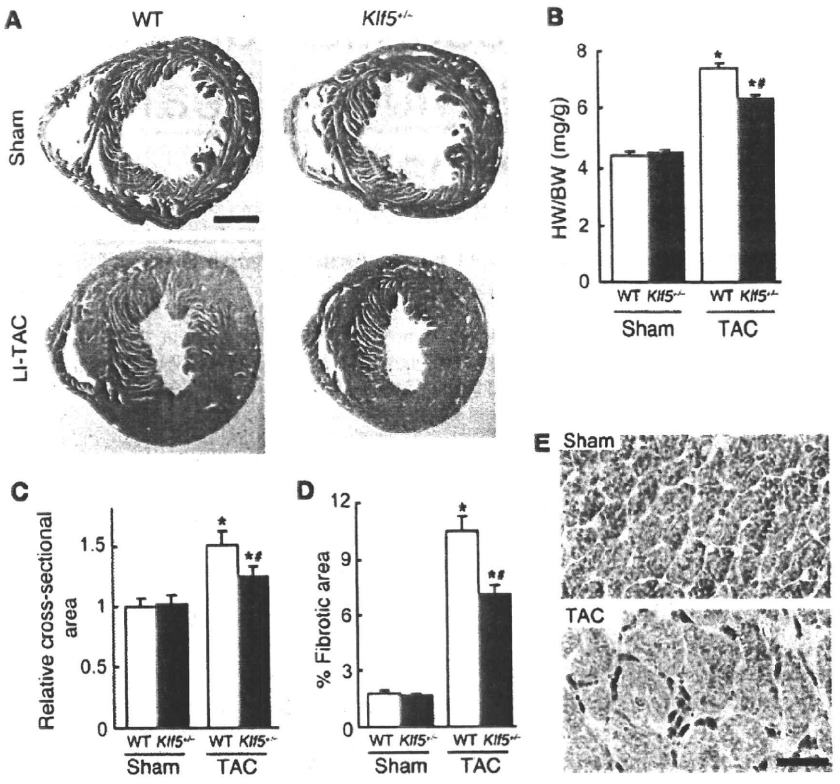

Figure 1
KLF5 is essential for pressure overload–induced hypertrophy. (**A–D**) *Klf5*$^{+/-}$ and wild-type mice were subjected to LI-TAC or sham operation. (**A**) Representative low-magnification views of H&E-stained heart sections from WT and *Klf5*$^{+/-}$ mice 2 weeks after the operations. Scale bar: 1 mm. (**B** and **C**) Heart weight/body (HW/BW) weight ratios (**B**) and relative cross-sectional areas of cardiomyocytes (**C**) from wild-type and *Klf5*$^{+/-}$ hearts. (**D**) Fractional areas of fibrosis in cross sections of hearts as determined by elastic picrosirius red staining. $^{*}P < 0.01$ versus sham control of the same genotype; $^{\#}P < 0.05$ versus wild-type subjected to TAC. $n = 7$. (**E**) Expression of KLF5 in normal and hypertrophied hearts 4 days after LI-TAC. Cells were double stained for KLF5 (brown) and a cardiomyocyte marker, αMHC (red); nuclei were counterstained in blue. Scale bar: 20 μm.

to pressure overload, cardiac fibroblast–specific deletion of *Klf5* ameliorated cardiac hypertrophy in a moderate-intensity pressure overload model, indicating that fibroblasts are essential for hypertrophic responses of the myocardium. Notably, however, cardiac fibroblast–specific *Klf5*-knockout mice developed severe heart failure when subjected to high-intensity pressure overload, suggesting cardiac fibroblasts have a cardioprotective function. We further demonstrated that KLF5 controls expression of IGF-1, which mediates the interplay between cardiomyocytes and fibroblasts. These data provide compelling evidence that cardiac fibroblasts play a pivotal role in the adaptive response of the myocardium.

Results

KLF5 plays an important role in pressure overload–induced cardiac hypertrophy. To analyze KLF5's function in cardiac adaptive responses, we first established models of pressure overload–induced cardiac hypertrophy using transverse aortic constriction (TAC). By applying a low-intensity TAC (LI-TAC) for 2 weeks, we were able to induce cardiac hypertrophy with preserved cardiac systolic function, while application of high-intensity TAC (HI-TAC) induced severe myocardial dysfunction and LV dilation (Supplemental Figures 1 and 2; supplemental material available online with this article; doi:10.1172/JCI40295DS1). The survival rates in the LI- and HI-TAC groups were 100% and 90%, respectively, after 2 weeks, which suggests that the LI-TAC model induces adaptive hypertrophy, while in the HI-TAC model, the adaptive response fails to protect against the severe pressure overload and enable maintenance of cardiac function.

When we examined the involvement of KLF5 in cardiac hypertrophy using the LI-TAC model, we found that cardiac expression of KLF5 was increased by LI-TAC (Supplemental Figure 3) and that LI-TAC–induced cardiac hypertrophy and fibrosis was diminished in *Klf5*$^{+/-}$ mice (Figure 1 and Supplemental Figure 4). Moreover, expression of 4 fibrosis-related genes, *Col1a1*, *Fn1*, *Ctgf*, and *Spp1*, was significantly suppressed in *Klf5*$^{+/-}$ mice (Supplemental Figure 4). Thus KLF5 appears to play a critical role in pressure overload–induced cardiac hypertrophy and fibrosis.

Cardiomyocyte-specific deletion of Klf5 does not affect pressure overload–induced cardiac hypertrophy. We found that *Klf5* is mainly expressed in fibroblasts (Supplemental Figure 3C), which suggests that its function in fibroblasts might contribute to the phenotypes seen in *Klf5*$^{+/-}$ mice. To test this idea, we generated several conditional *Klf5*-knockout mouse lines (Supplemental Figure 5). Homozygous *Klf5*-floxed (*Klf5*$^{fl/fl}$) mice appeared normal, and expression of *Klf5* was unaltered (data not shown). The *Klf5*$^{fl/fl}$ mice were then crossed with cardiomyocyte-specific Cre transgenic mice (*αMHC-Cre*) (20). In cardiomyocytes from adult cardiomyocyte-specific *Klf5*-knockout (*Klf5*$^{fl/fl}$;*αMHC-Cre*) mice, which were homozygous for both floxed *Klf5* and the *αMHC-Cre* transgene, approximately 70% of the *Klf5* gene was deleted (Supplemental Figure 6). When *Klf5*$^{fl/fl}$;*αMHC-Cre* mice and control *Klf5*$^{fl/fl}$ mice were subjected to LI-TAC, there were no differences in cardiac structure or function, or gene expression, between the 2 groups (Figure 2 and Supplemental Figure 7), which means that the level of *Klf5* deletion obtained in *Klf5*$^{fl/fl}$;*αMHC-Cre* mice did not affect the hypertrophic response to TAC.

Cardiac fibroblast–specific deletion of Klf5 reduces hypertrophic and fibrotic responses. We then analyzed the function of KLF5 in cardiac fibroblasts using a transgenic mouse line in which Cre recombinase was driven by a 3.9-kb mouse *Postn* promoter (21, 22), which is restricted to the non-myocyte lineage in the neonatal heart (P. Snider and S.J. Conway, unpublished observations). Periostin, which is encoded by *Postn*, is not normally expressed in either the

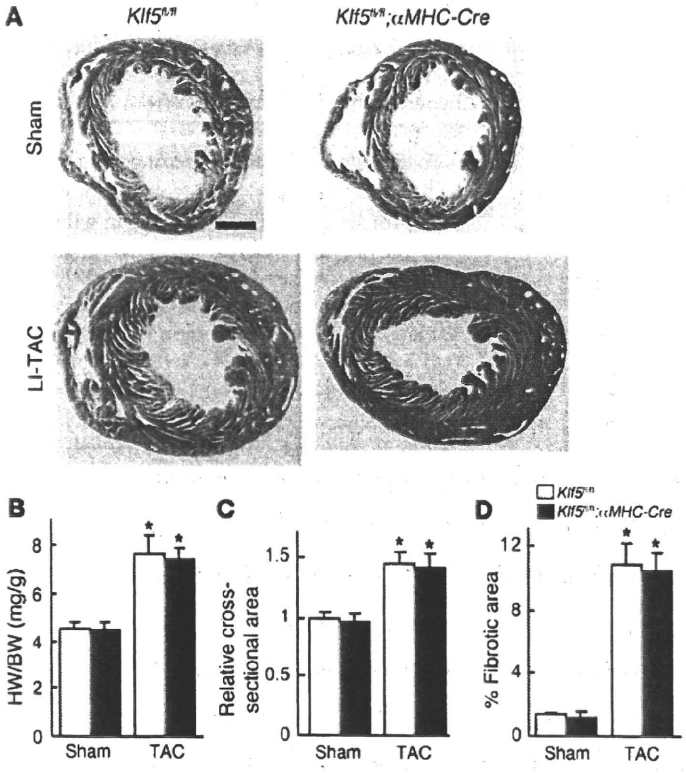

Figure 2

Cardiomyocyte-specific deletion of *Klf5* did not alter pressure overload–induced hypertrophy. *Klf5*$^{fl/fl}$ and *Klf5*$^{fl/fl}$;*αMHC-Cre* mice were subjected to LI-TAC or sham operation. (**A**) Representative low-magnification views of H&E-stained heart sections 2 weeks after LI-TAC. Scale bar: 1 mm. (**B** and **C**) Heart weight/body weight ratios (**B**) and relative cross-sectional areas of cardiomyocytes normalized to those obtained from *Klf5*$^{fl/fl}$ mice subjected to sham operations (**C**). (**D**) Fractional areas of fibrosis. **P* < 0.01 versus sham control of the same genotype. *n* = 7.

normal or pathological cardiomyocyte lineage (23), but is induced in cardiac fibroblasts by TAC (9, 24, 25). The activity of Cre recombinase in the *Postn-Cre* mice was examined after they were crossed with *R26RstoplacZ* indicator mice (26). Although only a few β-galactosidase$^+$ cells were found in the heart under basal conditions, LI-TAC induced robust *lacZ* expression in fibrotic areas in hearts from *R26RstoplacZ;Postn-Cre* mice (Figure 3A and Supplemental Figure 8). As expected, *lacZ* expression was not detected in either cardiomyocytes or ECs (Supplemental Figure 8).

We then used flow cytometry to further analyze expression of β-galactosidase in populations enriched in either cardiomyocytes or non-myocytes isolated from *R26RstoplacZ;Postn-Cre* mice subjected to LI-TAC (Supplemental Figure 9). β-Galactosidase$^+$ cells were not found in the cardiomyocyte population. Moreover, β-galactosidase$^+$ cells isolated from the non-myocyte population expressed a fibroblast-specific marker, discoidin domain receptor 2 (*Ddr2*), but not the cardiomyocyte-specific marker αMHC (*Myh6*) or the endothelial marker VE-cadherin (*Cdh5*), which supports the notion that β-galactosidase$^+$ cells are fibroblasts.

Klf5$^{fl/fl}$ mice were then bred with the *Postn-Cre* mice to generate *Klf5*$^{fl/fl}$;*Postn-Cre* mice. These animals were born with no apparent abnormalities and were healthy into adulthood. To examine the efficacy of Cre-mediated deletion of *Klf5* in each cell type, we isolated cardiomyocytes, cardiac fibroblasts, and ECs from adult mice. Cardiomyocytes were isolated using the Langendorff perfusion method (27). Fibroblasts and ECs were sorted from non-myocyte-enriched cell populations using anti-Thy1 antibody for fibroblasts (11, 28) and anti-CD31 for ECs. Because Thy1 is also expressed in T lymphocytes, CD3$^-$ cells were analyzed for surface expression of Thy1 and CD31 (Figure 3B). When the mRNA expression of cell type–specific lineage markers was analyzed, *Myh6* was found to be expressed only in cardiomyocytes, while *Ddr2* was expressed only in Thy1$^+$CD31$^-$CD3$^-$ cells and *Cdh5* only in Thy1$^-$CD31$^+$CD3$^-$ cells (Figure 3C), which indicates that Thy1$^+$CD31$^-$CD3$^-$ cells were fibroblasts. Approximately 72% of the *Klf5* gene was deleted in Thy1$^+$CD31$^-$CD3$^-$ fibroblasts isolated from *Klf5*$^{fl/fl}$;*Postn-Cre* mice subjected to LI-TAC for 2 weeks, whereas only 4% was deleted in the sham-operated mice (Figure 3D). No *Klf5* deletion was observed in cardiomyocytes or ECs. Moreover, *Cre* mRNA was selectively expressed in Thy1$^+$ fibroblasts, as was endogenous *Postn* mRNA, which is consistent with fibroblast-specific Cre-mediated deletion by *Postn-Cre* (Supplemental Figure 10).

We further analyzed expression of *Klf5* mRNA in each cell type in mice subjected to either the sham operation or LI-TAC (Figure 3E). In sham-operated hearts, levels of *Klf5* expression were higher in Thy1$^+$ fibroblasts than in cardiomyocytes or ECs and did not differ between *Klf5*$^{fl/fl}$ and *Klf5*$^{fl/fl}$;*Postn-Cre* mice. LI-TAC markedly increased *Klf5* expression in fibroblasts (approximately 4-fold) and moderately increased it in cardiomyocytes in *Klf5*$^{fl/fl}$ mice. While *Klf5* expression was clearly reduced in fibroblasts from *Klf5*$^{fl/fl}$;*Postn-Cre*, as compared with *Klf5*$^{fl/fl}$ mice, it was not altered in cardiomyocytes, which is again consistent with fibroblast-specific deletion of *Klf5*.

LI-TAC induced less cardiac interstitial fibrosis in *Klf5*$^{fl/fl}$;*Postn-Cre* mice than in control *Klf5*$^{fl/fl}$ mice, as expected (Figure 4, A–C), and expression of fibrosis-related factors such as *Col1a1*, *Fn1*, *Ctgf*, and *Spp1* was reduced (Supplemental Figure 11A). In addition to fibrosis, increases in heart weight/body weight ratios, echocardiographic LV wall thickness, and cardiomyocyte cross-sectional area were smaller in *Klf5*$^{fl/fl}$;*Postn-Cre* mice than *Klf5*$^{fl/fl}$ mice (Figure 4, D–F). Moreover, expression levels of hypertrophy-related genes such as *Nppa*, which encodes atrial natriuretic peptide (ANP), and *Myh7*, which encodes β-myosin heavy chain, were lower in *Klf5*$^{fl/fl}$;*Postn-Cre* than *Klf5*$^{fl/fl}$ mice (Figure 4G), indicating suppression of hypertrophic responses. These phenotypes clearly demonstrate that not only is KLF5 expressed in cardiac fibroblasts essential for fibrosis, it is also important for mediating subsequent cardiomyocyte hypertrophy.

IGF-1 controlled by KLF5 mediates hypertrophic responses. We next investigated the mechanisms by which KLF5 expressed in fibroblasts controls hypertrophy of cardiomyocytes. Because earlier studies have suggested there are paracrine interactions between cardiomyocytes and fibroblasts (2, 3), we hypothesized that KLF5 might directly control the expression of paracrine factors in fibroblasts. To test that idea, we cultured cardiomyocytes in medium conditioned by cardiac fibroblasts transfected with either siRNA against KLF5 (29) or control siRNA (Figure 5A). We found that the medium conditioned by KLF5 knockdown fibroblasts was

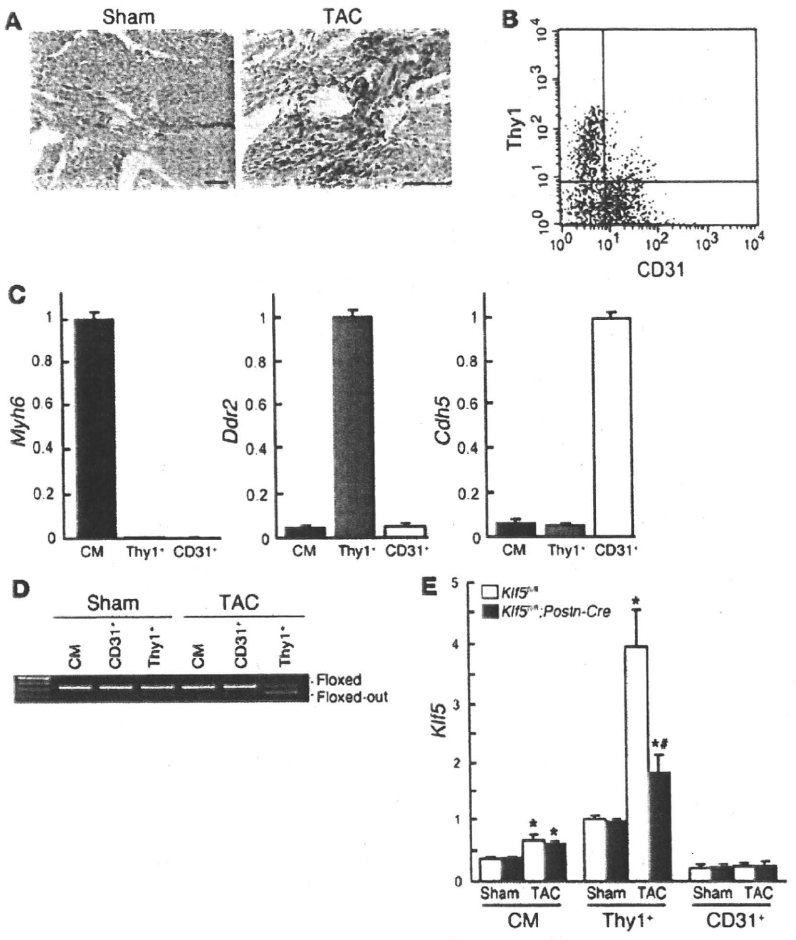

Figure 3

Fibroblast-specific deletion of *Klf5* in *Klf5$^{fl/fl}$;Postn-Cre* mice. (**A**) Fibroblast-specific deletion of the floxed region in *Postn-Cre* mice was examined using *R26RstoplacZ* indicator mice. *LacZ* expression was visualized using X-gal. Scale bars: 100 μm. (**B**) CD3$^-$ cells within non-myocyte-enriched cell populations isolated from adult hearts were analyzed for surface expression of the fibroblast marker Thy1 and the endothelial marker CD31. (**C**) Relative expression levels of cell-lineage markers in adult cardiomyocytes (CM) isolated using the Langendorff perfusion method, and in Thy1$^+$CD31$^-$CD3$^-$ (Thy1$^+$) and Thy1$^-$CD31$^+$CD3$^-$ (CD31$^+$) cells sorted from non-myocyte-enriched populations as shown in **B**. *Myh6* (encoding αMHC), *Ddr2* (encoding discoidin domain receptor 2), and *Cdh5* (encoding VE-cadherin) were used as markers for cardiomyocytes, fibroblasts, and ECs, respectively. The cells were isolated from 8-week-old mice subjected to sham operations. (**D**) Competitive PCR analysis for quantitation of Cre-mediated recombination of the *Klf5* gene region in adult cardiomyocytes, CD31$^+$ ECs, and Thy1$^+$ fibroblasts isolated from *Klf5$^{fl/fl}$* and *Klf5$^{fl/fl}$;Postn-Cre* mice 2 weeks after either the sham or LI-TAC operation. Competitive PCR was performed as shown in Supplemental Figure 6B. (**E**) Relative expression levels of *Klf5* mRNA in adult cardiomyocytes, Thy1$^+$ fibroblasts, and CD31$^+$ ECs isolated from *Klf5$^{fl/fl}$* and *Klf5$^{fl/fl}$;Postn-Cre* mice as shown in **B** 5 days after either sham operation or LI-TAC. Expression levels of *Klf5* mRNA were assessed using real-time PCR and normalized to those of 18s rRNA, after which they were further normalized to the levels in Thy1$^+$ cells isolated from *Klf5$^{fl/fl}$* mice subjected to the sham operation. *$P < 0.01$ versus sham control of the same genotype in the same cell lineage group; #$P < 0.01$ versus *Klf5$^{fl/fl}$* mice subjected to LI-TAC in the same cell lineage group.

less able to induce cardiomyocyte hypertrophy and ANP secretion than medium conditioned by control cells (Figure 5, B–D), suggesting that, in fibroblasts, KLF5 does indeed control production of paracrine factors that induce hypertrophic responses in cardiomyocytes. Similarly, Thy1$^+$ cardiac fibroblasts isolated from *Klf5$^{fl/fl}$;Postn-Cre* mice subjected to LI-TAC were less able to induce cardiomyocyte hypertrophy than Thy1$^+$ cells from *Klf5$^{fl/fl}$* mice (Supplemental Figure 12).

To identify the paracrine factor genes targeted by KLF5, we compared genome-wide gene expression profiles for the left ventricle in wild-type mice subjected to the sham operation and those subjected LI-TAC; and in *Klf5$^{fl/fl}$* and *Klf5$^{fl/fl}$;Postn-Cre* mice subjected to LI-TAC (Supplemental Table 1). Thereafter, expression levels were verified by real-time PCR. We screened for genes encoding secreted proteins whose expression levels were significantly increased by LI-TAC in wild-type mice and were lower in *Klf5$^{fl/fl}$;Postn-Cre* than *Klf5$^{fl/fl}$* mice. Among the 11 genes that met these criteria, 6 were preferentially expressed in cardiac fibroblasts, as compared with cardiomyocytes (Supplemental Table 1), and included 2 growth factor genes, *Igf1* and *Tgfb3*, encoding IGF-1 and TGF-β3, and *Postn*, encoding periostin. While knocking down KLF5 significantly reduced expression of *Igf1* in cultured fibroblasts (Figure 6A), expression levels of *Tgfb3* and *Postn* were not altered (Supplemental Figure 13), suggesting that KLF5 might directly control *Igf1* transcription. Moreover, *Igf1* expression was highly enriched in fibroblasts (Figure 6B). IGF-1 reportedly promotes cardiac growth and improves cardiac function in patients with LV dysfunction and advanced heart failure (30–32). We therefore further analyzed *Igf1* as a likely downstream target of KLF5.

We found that upregulation of myocardial *Klf5* expression after LI-TAC preceded the induction of *Igf1* (Figure 6C). Levels of both *Klf5* and *Igf1* expression were reduced in *Klf5$^{fl/fl}$;Postn-Cre* mice, as compared with those in *Klf5$^{fl/fl}$* mice, during the 2-week observation period following the LI-TAC operation. The *Igf1* promoter contains a KLF-binding motif (CCCCACCCAC) at -53 bp, which, in the rat, is reportedly important for promoter activity and bound by an as-yet-unidentified transcription factor (Figure 6D) (33). Reporter analysis of the *Igf1* promoter showed that KLF5 transactivated this promoter, but KLF15, which is expressed in cardiomyocytes and cardiac fibroblasts (34, 35), failed to do so, and mutation within the potential KLF5-binding motif abolished KLF5-dependent transactivation (Figure 6D). ChIP assays confirmed that KLF5 bound to the *Igf1* promoter (Figure 6E). As reported (30–32), IGF-1 induced hypertrophy in cultured cardiomyocytes (Supplemental Figure 14A), and inhibition of IGF-1 using a neutralizing antibody significantly suppressed cardiomyocyte hypertrophy induced by the fibroblast-conditioned medium (Figure 6F). Taken together, the results so far demonstrate that KLF5 directly regulates expression of *Igf1*, which appears to be a major cardiotrophic factor secreted by fibroblasts.

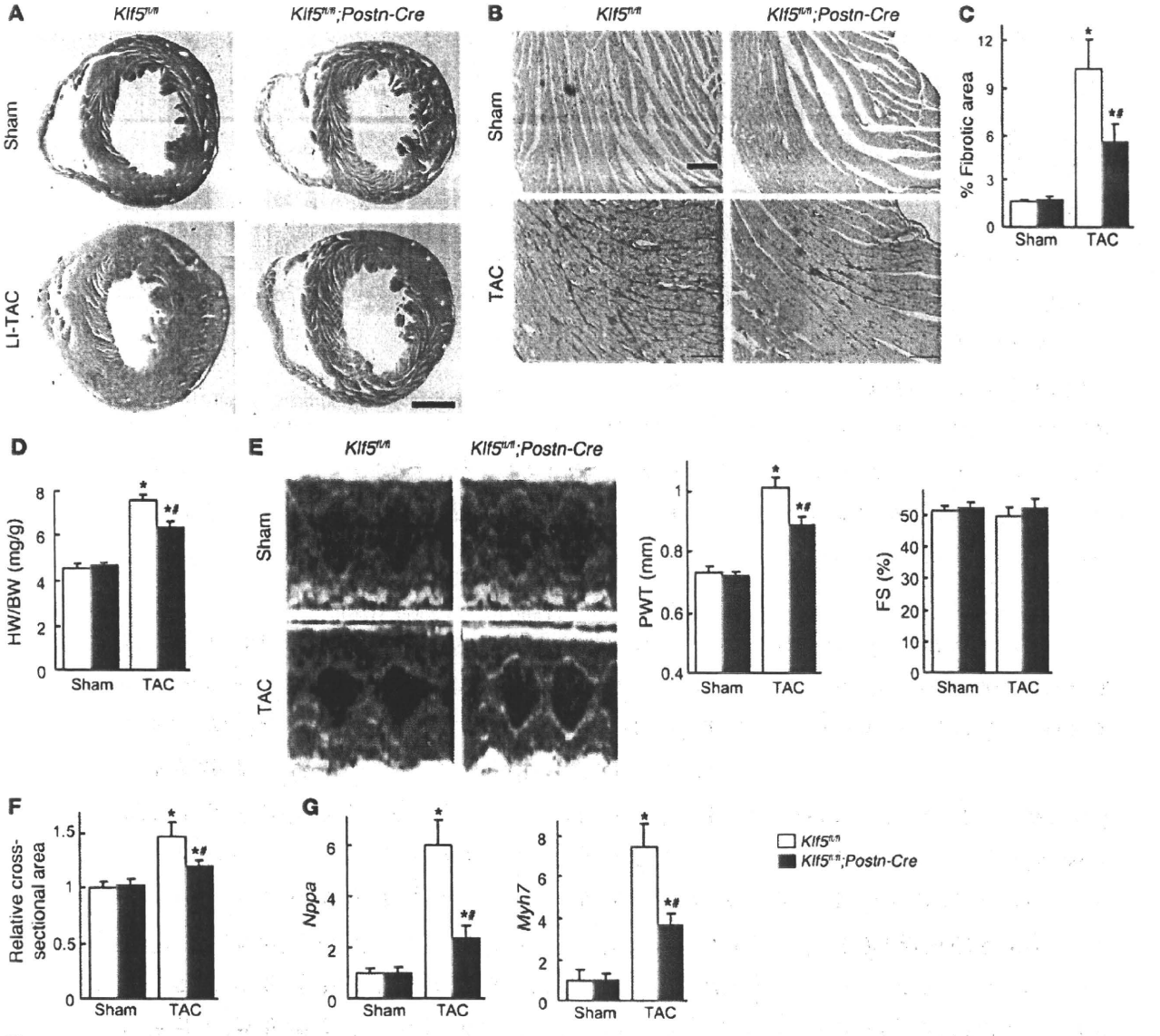

Figure 4

Fibroblast-specific deletion of *Klf5* attenuates cardiac hypertrophy and fibrosis after TAC. *Klf5*$^{fl/fl}$ and *Klf5*$^{fl/fl}$;*Postn-Cre* mice were subjected to LI-TAC or sham operation. (**A**) Representative low-magnification views of H&E-stained heart sections 2 weeks after the operations. Scale bar: 1 mm. The bottom-left panel was composited from 2 photographs of the same section. (**B**) Representative elastic picrosirius red–stained sections and fibrotic areas. Scale bars: 100 μm. (**C**) Fibrotic areas. (**D**) Heart weight/body weight ratios 2 weeks after the operations. (**E**) Echocardiographic analysis 2 weeks after the operations. (**F**) Relative cross-sectional areas of cardiomyocytes. (**G**) Relative expression levels of *Nppa* and *Myh7* mRNA. Expression levels of each gene were normalized to 18s ribosomal RNA levels and then further normalized with respect to those obtained with samples from *Klf5*$^{fl/fl}$ mice subjected to sham operation. $^{*}P < 0.01$ versus sham control of the same genotype; $^{\#}P < 0.01$ versus *Klf5*$^{fl/fl}$ subjected to TAC. $n = 7$.

We also found that the numbers of fibroblasts positive for BrdU incorporation following LI-TAC were significantly smaller in *Klf5*$^{fl/fl}$;*Postn-Cre* hearts than *Klf5*$^{fl/fl}$ hearts (Supplemental Figure 11B), which suggests that KLF5 may also be involved in modulating fibroblast proliferation, either autonomously (36–38) or by regulating autocrine/paracrine factors. Consistent with the latter, we found that IGF-1 induces fibroblast proliferation (Supplemental Figure 14B).

We previously reported that KLF5 also controls *Pdgfa*, which encodes PDGF-A, in response to angiotensin II (14, 39). At the same concentrations, PDGF-A was less able to induce cardiomyocyte hypertrophy than IGF-1 (Supplemental Figure 14A), though PDGF-A and IGF-1 similarly induced fibroblast proliferation (Supplemental Figure 14B). PDGF-A induced greater migration of fibroblasts in Boyden chamber assays than IGF-1 (Supplemental Figure 14C), suggesting PDGF-A is primarily involved in mediating the migration and proliferation of fibroblasts. Thus, among the paracrine factors controlled by KLF5, it appears to be a change in IGF-1 activity that is primarily responsible for the reduced cardiac hypertrophy observed in LI-TAC *Klf5*$^{fl/fl}$;*Postn-Cre* hearts.

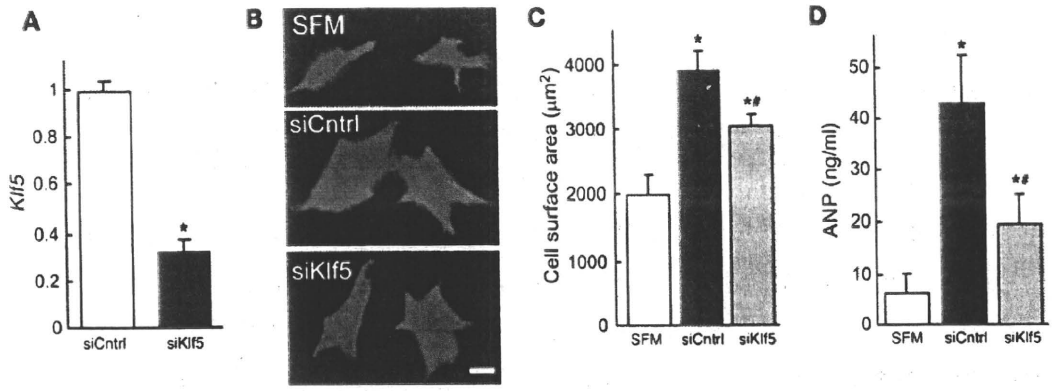

Figure 5

KLF5 controls expression of paracrine factors in cardiac fibroblasts that mediate cardiomyocyte hypertrophy. (**A**) siRNA-mediated knockdown of *Klf5* in cardiac fibroblasts. *Klf5* levels were normalized to those in cells transfected with the control siRNA (siCntrl). **P* < 0.01 versus siCntrl. (**B–D**) Cultured cardiomyocytes were incubated with serum-free medium (SFM) or conditioned medium prepared from cardiac fibroblasts transfected with control or *Klf5* siRNA for 48 hours. (**B**) Representative cardiomyocytes are shown stained for sarcomeric α-actinin (green) and nuclei (Hoechst 33258, blue). Scale bar: 10 μm. (**C**) Cell surface areas of 100 cells from each group. **P* < 0.01 versus cells treated with SFM; #*P* < 0.05 versus cells treated with medium conditioned by siCntrl transfectants. (**D**) ANP concentrations in culture medium conditioned by cardiomyocytes. **P* < 0.05 versus SFM; #*P* < 0.05 versus siCntrl.

Cardiac fibroblasts are essential for adaptive responses to severe pressure overload. Next we assessed the importance of cardiac fibroblasts in the adaptive responses of the myocardium for maintenance of cardiac function. *Klf5*$^{fl/fl}$ and *Klf5*$^{fl/fl}$*;Postn-Cre* mice were subjected to HI-TAC, which we previously found to induce cardiac dysfunction within 2 weeks (Supplemental Figures 1 and 2). After 10 days of HI-TAC, *Klf5*$^{fl/fl}$*;Postn-Cre* mice were visibly emaciated, and their body weights were correspondingly diminished (data not shown). In addition, mortality among *Klf5*$^{fl/fl}$*;Postn-Cre* mice was significantly higher than among *Klf5*$^{fl/fl}$ mice after 14 days of HI-TAC (Figure 7A). Pulmonary edema and/or hemorrhage were noted in most of the dead *Klf5*$^{fl/fl}$*;Postn-Cre* mice, and even in those that survived, lung weights were significantly increased due to pulmonary congestion and alveolar edema (Figure 7, B and C). Many *Klf5*$^{fl/fl}$*;Postn-Cre* mice also exhibited shallow, rapid breathing characteristic of heart failure. Nonetheless, cardiac hypertrophy and fibrosis were markedly attenuated in *Klf5*$^{fl/fl}$*;Postn-Cre* mice, though LV luminal diameters were markedly increased (Figure 7, D–G). Because of the fragility of *Klf5*$^{fl/fl}$*;Postn-Cre* mice, systematic echocardiographic analysis could not be performed, as even a minimum dose of anesthetic was lethal. However, the 1 *Klf5*$^{fl/fl}$*;Postn-Cre* mouse that survived the anesthesia showed marked LV dilation and diminished systolic function (Figure 7H). Apparently, expression of KLF5 by cardiac fibroblasts is necessary for the adaptive and protective activities that take place within the myocardium in response to severe pressure overload.

Finally, we tested whether IGF-1 is required for the cardioprotective responses to pressure overload by using JB1, a peptide IGF-1 receptor antagonist, to inhibit IGF-1 signaling in vivo (40). JB1 did not affect survival, cardiac function, heart weights, or cardiac histology in sham-operated control mice (data not shown). In mice subjected to HI-TAC, by contrast, JB1 administration led to the emaciation and shallow, rapid breathing characteristic of heart failure as well as early death (Figure 8A). In JB1-treated mice subjected to HI-TAC, the lung weights were significantly increased (Figure 8, B and C), cardiac hypertrophy was attenuated (Figure 8, D–F), and the left ventricle was significantly enlarged (Figure 8, D and F). Moreover, systolic function was impaired more than in vehicle-treated mice (Figure 8F), indicating that JB1 exacerbated the heart failure. IGF-1 secreted from cardiac fibroblasts thus appears to be a crucial mediator of the cardioprotective response to severe pressure overload.

Discussion

The results of the present study clearly demonstrate that cardiac fibroblasts play essential roles in cardioprotection and cardiomyocyte hypertrophy, at least in part by producing paracrine factors, including IGF-1. Based on the observation that in addition to extracellular matrix proteins, cardiac fibroblasts produce a variety of paracrine factors – some of which can induce hypertrophic responses in vitro – it has been postulated that an interplay between cardiomyocytes and fibroblasts is involved in cardiac hypertrophy and pathology (2, 3). However, the potential requirement for fibroblasts in the cardiac response to pathological stress in vivo has not been fully appreciated. Our study provides clear evidence that cardiac fibroblasts functionally contribute to the adaptive response to pressure overload in vivo. Particularly noteworthy is our finding that cardiac fibroblasts are absolutely required for protection of cardiac function in severe pressure overload. This means that cardiac fibroblasts are not mere bystanders acting only in fibrosis, but are crucial mediators of myocardial hypertrophy and adaptive responses in the heart. It was recently suggested that inappropriate angiogenesis plays an important role in heart failure (41). That finding, together with those summarized here, highlights the importance of the activities of the non-muscle cells residing in the myocardial interstitium. In addition to contributing to pathological remodeling, it is likely that these cells mediate homeostatic responses to physiological stress.

Our findings also indicate that KLF5 expressed in cardiac fibroblasts is a key regulator controlling the stress response in the myocardium. Moreover, the results obtained with cardiac fibroblast-specific *Klf5*-knockout mice suggest that IGF-1 produced by fibroblasts is also important for protective responses. These findings are consistent with the results of earlier studies of the effects

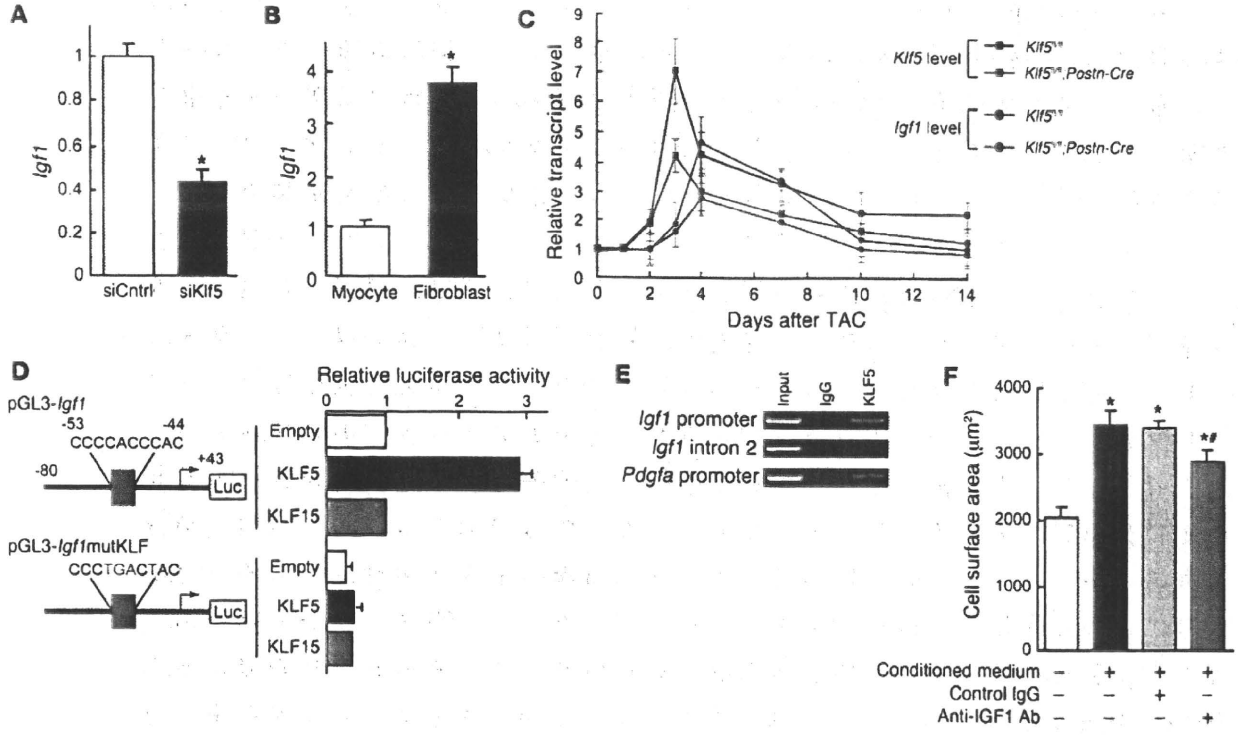

Figure 6

KLF5 transactivates the *Igf1* promoter. (**A**) KLF5 knockdown reduced *Igf1* expression in cardiac fibroblasts. KLF5 was knocked down as shown in Figure 5A. **P* < 0.01 versus siCntrl. (**B**) Fibroblast-selective expression of *Igf1*. *Igf1* mRNA levels in cultured cardiac fibroblasts were normalized to those of 18s rRNA and then further normalized with respect to those in cardiomyocytes. **P* < 0.01 versus cardiomyocytes. (**C**) Cardiac expression of *Klf5* and *Igf1* mRNA after LI-TAC in *Klf5*$^{fl/fl}$ and *Klf5*$^{fl/fl}$;*Postn-Cre* mice. Expression levels were normalized to those of 18s rRNA and then further normalized with respect to those in the hearts before TAC. (**D**) Reporter analysis of KLF5-depedent transactivation of the *Igf1* promoter. Luciferase reporter constructs driven by the wild-type *Igf1* promoter or a mutant promoter in which the potential KLF-binding site was mutated were cotransfected with either empty vector or a vector harboring *Klf5* or *Klf15*. Data are representative of 3 independent experiments. (**E**) ChIP assays of KLF5 binding to the *Igf1* and *Pdgfa* promoters. An intronic region of *Igf1* that does not contain a KLF-binding motif served as a negative control. (**F**) Effects of neutralizing IGF-1 on the cardiotrophic activity of fibroblast-conditioned medium. An antibody against IGF-1 (30 μg/ml) or normal IgG was added to the conditioned medium, after which the effect of the medium on cardiomyocyte surface area was analyzed. **P* < 0.01 versus cells treated with SFM; #*P* < 0.01 versus cells treated with fibroblast-conditioned medium.

of transgenic overexpression of IGF-1 and IGF-1 receptor in cardiomyocytes, which were also suggestive of IGF-1's role in physiological hypertrophy and cardiac protection (42–46). Thus IGF-1 produced locally by fibroblasts appears to be a key mediator of cardiac hypertrophy and myocardial protection against pressure overload.

The present study identified *Igf1* as the target of KLF5 in fibroblasts involved in the cardiac adaptive response. However, KLF5 also likely controls the expression of genes other than *Igf1* and *Pdgfa*, including those encoding paracrine factors involved in regulating fibroblast function (Supplemental Table 1). We would therefore expect future studies of the gene networks controlled by KLF5 in cardiac fibroblasts to shed additional light on their homeostatic and pathological functions. In that regard, it will also be important to analyze the possible interplay between KLF5 and other members of the KLF family. Previous studies have demonstrated the functional roles played by several KLFs in the heart (34, 35, 47, 48). For instance, KLF15 negatively regulates cardiac fibrosis (34). It is therefore conceivable that networks of KLFs contribute to the myocardial responses to stress. Finally, our results suggest that therapeutic modulation of cardiac fibroblast function may represent a novel approach to the prevention and/or treatment of heart failure.

Methods

For experimental procedures not described herein, see Supplemental Methods.

Animals. Mice were housed in temperature-controlled rooms with a 12-hour light/12-hour dark cycle. All experiments were approved by the University of Tokyo Ethics Committee for Animal Experiments and strictly adhered to the guidelines for animal experiments of the University of Tokyo.

Generation of Klf5-floxed mice. A 12-kb *Klf5* fragment containing exons 1–3 was used to construct the targeting vector. The scheme for construction of the targeting vectors is shown in Supplemental Figure 5. The targeting construct was introduced into ES cells by electroporation, and G418-resistant clones were then examined for homologous recombination using Southern blot analysis with appropriate 3′ probes. Six ES clones that contained the correctly targeted *Klf5* locus were obtained, and 2 were injected into 129/Sv blastocysts to obtain chimeric mice. Male chimeras were bred with female transgenic mice expressing the enhanced site-specific recombinase FLP to remove the FRT-flanked neomycin cassette to generate heterozygous floxed *Klf5* (*Klf5*$^{fl/+}$) mice. *Klf5*$^{fl/+}$ mice were then backcrossed with C57BL/6 mice using the marker-assisted speed congenic method (49). The mice were genotyped by Southern blot analysis or PCR. Southern blot analysis was performed after *Hind*III digestion using a 396-bp PCR-amplified

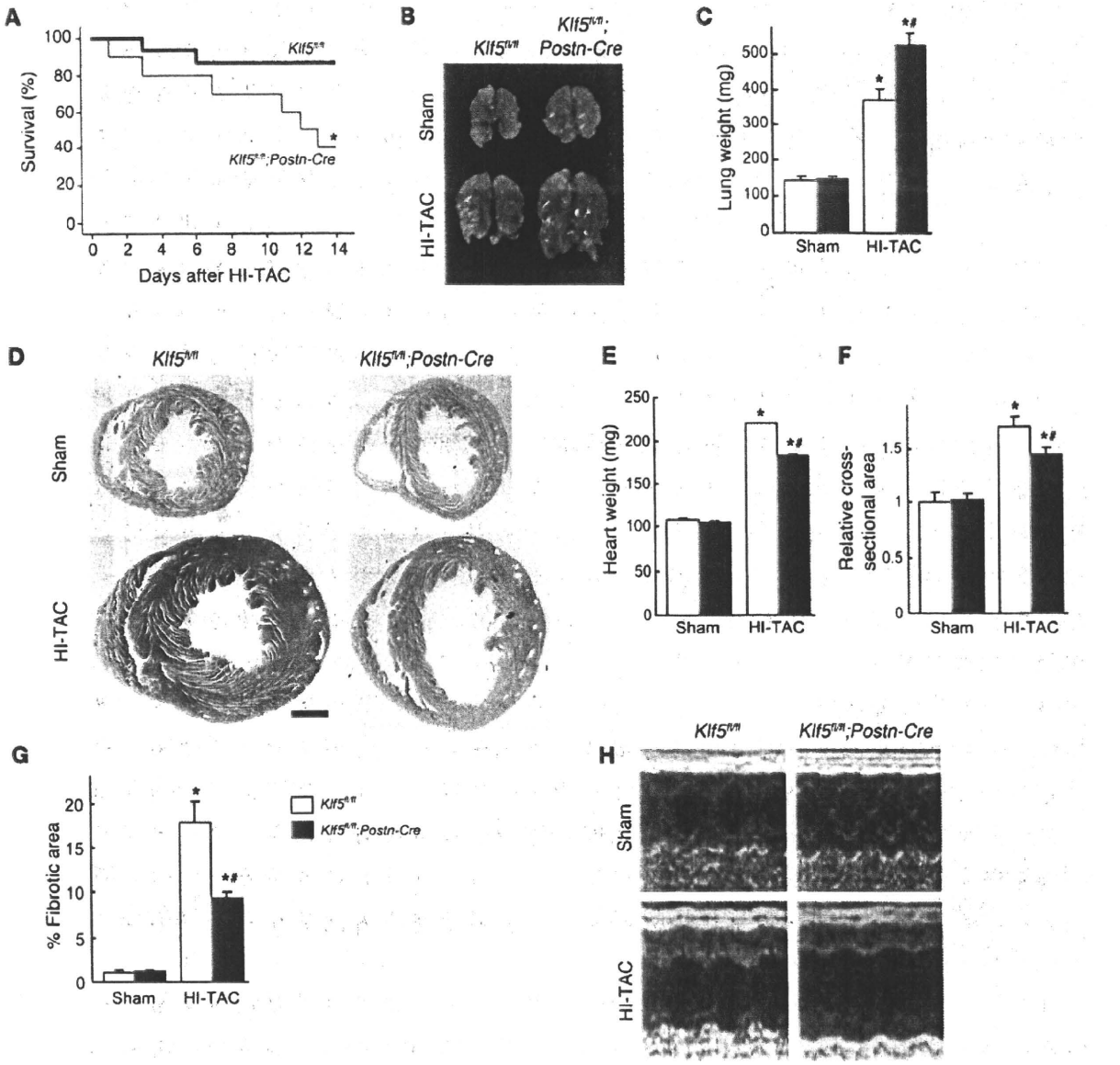

Figure 7

Cardiac fibroblasts are essential for the protective response elicited by severe pressure overload. (**A–H**) *Klf5*$^{fl/fl}$ and *Klf5*$^{fl/fl}$;*Postn-Cre* mice were subjected to HI-TAC or sham operation. (**A**) Kaplan-Meier survival analysis of *Klf5*$^{fl/fl}$ (n = 16) and *Klf5*$^{fl/fl}$;*Postn-Cre* (n = 10) mice after HI-TAC. *P < 0.05 versus *Klf5*$^{fl/fl}$. (**B**) Representative pictures of lungs 2 weeks after the operations. Note the severe lung edema in *Klf5*$^{fl/fl}$;*Postn-Cre* mice subjected to HI-TAC. (**C**) Lung weights in *Klf5*$^{fl/fl}$ (n = 5) and *Klf5*$^{fl/fl}$;*Postn-Cre* (n = 3) mice 2 weeks after the operations. (**D**) Representative low-magnification views of H&E-stained heart sections 2 weeks after the operations. Scale bar: 1 mm. (**E–G**) Heart weight/body weight ratios (**E**), relative cross-sectional areas of cardiomyocytes (**F**), and fibrotic areas (**G**) in *Klf5*$^{fl/fl}$ (n = 5) and *Klf5*$^{fl/fl}$;*Postn-Cre* (n = 3) mice 2 weeks after the HI-TAC operation. *P < 0.01 versus sham control of the same genotype; #P < 0.05 versus *Klf5*$^{fl/fl}$ mice subjected to HI-TAC. (**H**) M-mode echocardiographic tracings obtained 2 weeks after the operations.

probe for hybridization (Supplemental Figure 5). The probe for intron 1 was made by PCR using primers 5′-TGTCGTGGTGCTTTGAGAAG-3′ and 5′-TATCTTCCAGGCCCTGATTG-3′. PCR for genotyping was performed with primers A (5′-GCATCAGGAGGGTTTCATGT-3′) and B (5′-GTCTCGGCCTCATTGCTAAG-3′), which yielded 164-bp and 331-bp products for wild-type and floxed *Klf5* alleles, respectively.

Quantification of Cre-mediated recombination. Competitive PCR was performed to calculate the relative deletion frequency using primers A, B, and C (5′-TGACCCATTACCGAATCTACTG-3′), which produced 331-bp and 250-bp bands for the floxed and floxed-out *Klf5* alleles, respectively. The respective abundances of the floxed and floxed-out *Klf5* alleles were analyzed using real-time PCR with the same primer sets. To calculate absolute numbers of alleles in a given cell sample, we used external standards containing known numbers of DNA fragments derived from *Klf5*-floxed and floxed-out alleles.

TAC model. TAC was performed as described previously (50). Briefly, mice (8–10 weeks old, 21–24 g body weight) were anesthetized by intraperitoneal injection of a mixture of xylazine (5 mg/kg) and ketamine (100 mg/kg).

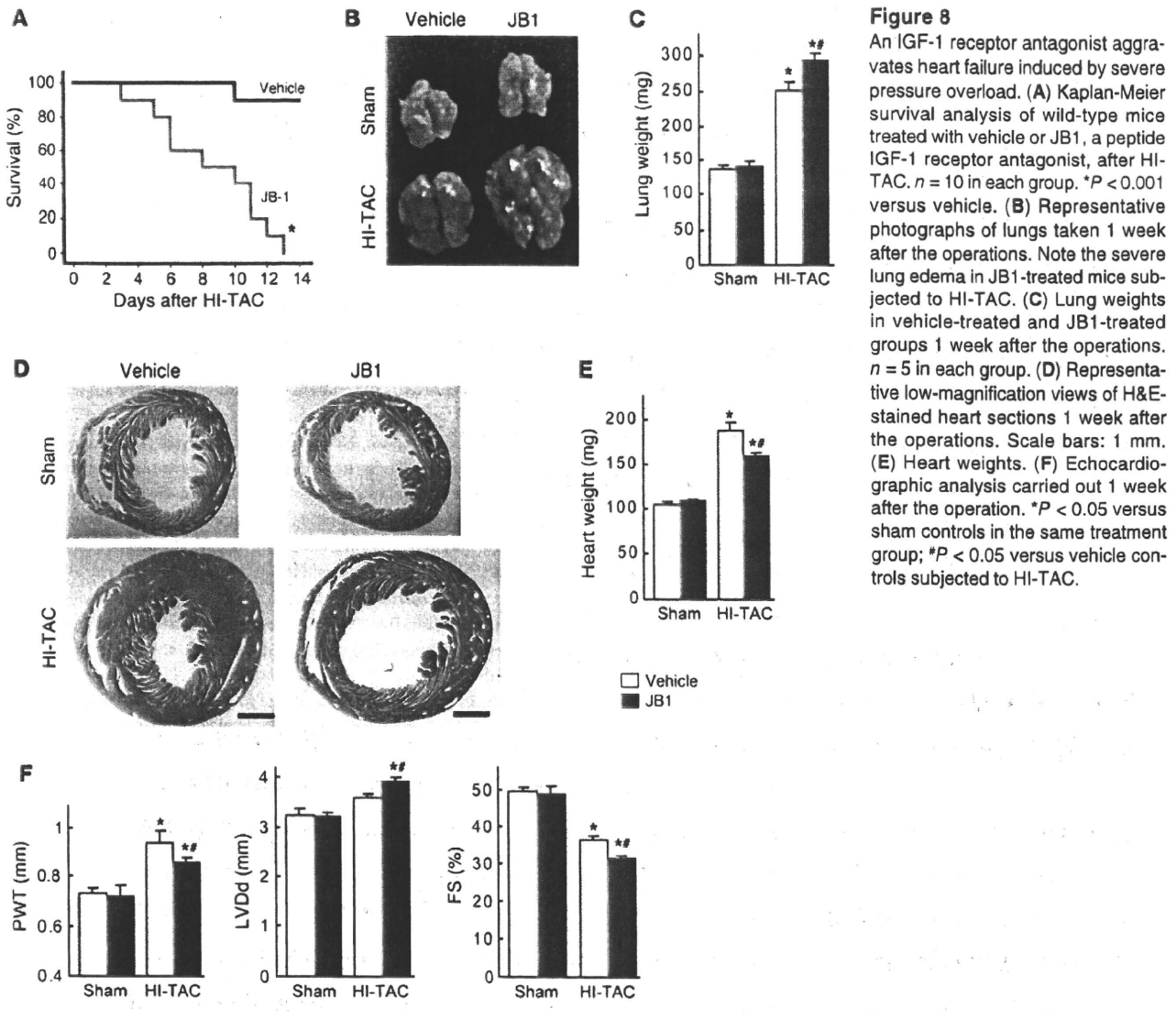

Figure 8
An IGF-1 receptor antagonist aggravates heart failure induced by severe pressure overload. (**A**) Kaplan-Meier survival analysis of wild-type mice treated with vehicle or JB1, a peptide IGF-1 receptor antagonist, after HI-TAC. $n = 10$ in each group. $^*P < 0.001$ versus vehicle. (**B**) Representative photographs of lungs taken 1 week after the operations. Note the severe lung edema in JB1-treated mice subjected to HI-TAC. (**C**) Lung weights in vehicle-treated and JB1-treated groups 1 week after the operations. $n = 5$ in each group. (**D**) Representative low-magnification views of H&E-stained heart sections 1 week after the operations. Scale bars: 1 mm. (**E**) Heart weights. (**F**) Echocardiographic analysis carried out 1 week after the operation. $^*P < 0.05$ versus sham controls in the same treatment group; $^\#P < 0.05$ versus vehicle controls subjected to HI-TAC.

The animals were then placed in a supine position, an endotracheal tube was inserted, and the animals were ventilated using a volume-cycled rodent ventilator with a tidal volume of 0.4 ml room air and a respiratory rate of 110 breaths/minute. The chest cavity was exposed by cutting open the proximal portion of the sternum. After the aortic arch between the innominate and left common carotid arteries was isolated, it was constricted with a 7-0 nylon suture tied firmly 3 times against a 25- or 27-gauge blunted needle for LI- and HI-TAC, respectively. Sham-operated mice underwent the identical surgical procedure, including isolation of the aorta, but without placement of the suture.

Administration of JB1, a peptide IGF-1 receptor antagonist. C57BL/6 mice (8–10 weeks old, 21–24 g body weight) were anesthetized by intraperitoneal injection of pentobarbital sodium (50 mg/kg). An incision was made in the midscapular region under sterile conditions, and an osmotic minipump (Alzet) containing either JB1 (BACHEM) dissolved in 0.15 mol/l NaCl and 1 mmol/l acetic acid or vehicle only was implanted. The delivery rate was 1 mg/kg/d for 14 days.

Echocardiography. Animals were lightly anesthetized with 2,2,2-tribromoethanol (200 mg/kg) and set in a supine position. Two dimensional (2D) guided M-mode echocardiography was performed using an echocardiogram (model 4500, Sonos) equipped with a 15 to 6 L MHz transducer (Philips). The heart at the level of the LV papillary muscle was imaged in the 2D mode in the parasternal short-axis view with a depth setting of 2 cm. LV diastolic posterior wall thickness (PWT), LV diastolic dimensions (LVDd), and LV end-systolic dimensions (LVDs) were measured. LV fractional shortening (%FS) was calculated as (LVDd - LVDs)/LVDd × 100.

Histological analysis. Heart sections were prepared as described previously (14) and stained with H&E for overall morphology. Immunohistochemical staining of KLF5 was performed using an anti-KLF5 monoclonal antibody (KM1784). A biotin-conjugated goat anti-rat antibody, streptavidin-conjugated horseradish peroxidase (Dako), and 3,3′-diaminobenzidine (DAB) were used to visualize labeling. For double staining of KLF5 and αMHC, we also used anti-αMHC monoclonal antibody CMA19 (51). Simple Stain AP(M) (Nichirei) and an Alkaline Phosphatase Substrate Kit I (Vector) were used to visualize labeling. To quantify cardiac interstitial fibrosis, we stained sections with elastic picrosirius red, after which images were captured with a digital camera and analyzed using Photoshop (Adobe) and Scion Image.

β-Galactosidase staining. Heart tissues were fixed for 12 hours at 4°C in PBS containing 0.4% glutaraldehyde, 0.01% Na deoxycholate, 0.1% NP40, 0.1 M $MgCl_2$, and 5 mM EGTA; rinsed 3 times for 30 minutes in PBS; and

then incubated for 24 hours at 37°C in a staining solution [1 mM $MgCl_2$, 20 mM $K_3Fe(CN)_6$, 20 mM $K_4Fe(CN)_6$, 1 mg/ml X-gal in PBS]. LacZ-stained sections were counterstained with nuclear fast red for nuclei, biotin-conjugated isolectin B4 (Vector) for ECs, and elastic picrosirius red for fibrosis.

Cardiomyocyte cross-sectional area. Heart sections were deparaffinized, rehydrated, and incubated for 1 hour at room temperature with FITC-labeled wheat germ agglutinin (Sigma-Aldrich) to visualize myocyte membranes. Regions that included the circular shapes of capillaries were selected from the epicardial side of the LV free walls. The mean cross-sectional area of cardiomyocytes was determined for each mouse from 60 to 80 cells.

RNA extraction and real-time PCR. Heart tissues were stored in RNAlater RNA stabilization reagent (QIAGEN) at 4°C. Total RNA was extracted using an RNeasy Fibrous Tissue Mini Kit (QIAGEN). First-strand cDNA synthesis was performed with 1 μg of total RNA, random hexamers, and SuperScript III Reverse Transcriptase (Invitrogen). Real-time PCR was performed using a QuantiTect SYBR Green PCR kit (QIAGEN) in a LightCycler (Roche). The expression level of each gene was normalized to that of 18s rRNA, which served as an endogenous internal control. The sequences of the PCR primers are shown in Supplemental Table 2.

Isolation of neonatal and adult cardiomyocytes and non-myocytes. Neonatal ventricles from 1-day-old ICR mice were separated and minced in ice-cold balanced salt solution, as described previously with minor modifications (52). To isolate cardiac cells, the tissues were incubated in a balanced salt solution containing 0.2% collagenase type 2 (Worthington Biochemical) for 6 minutes at 37°C with agitation. The digestion buffer was replaced 7 times, at which point the tissues were completely digested. The dispersed cells were incubated in 10-cm culture dishes for 80 minutes to remove non-myocytes. The unattached viable cells, which were rich in cardiomyocytes, were cultured on gelatin-coated dishes at 37°C in DMEM supplemented with 10% FBS and 10 μM cytosine 1-β-D-arabinofuranoside (Ara C) to inhibit fibroblast proliferation. Using this protocol, we consistently obtained cell populations containing at least 90%–95% cardiomyocytes. Non-myocyte cells that attached to the dishes were cultured in DMEM supplemented with 10% FBS and allowed to grow to confluence, then they were trypsinized and passaged at1:3. This procedure yielded cell cultures that were almost exclusively fibroblasts by the first passage. Experiments were carried out after 2 or 3 passages.

Adult cardiomyocytes were isolated using the Langendorff perfusion method as previously described (27). For isolation of non-myocyte-enriched cells, hearts were dissected free of vessels and atria, washed in ice-cold modified Krebs-Henseleit bicarbonate (KHB) buffer (pH 7.2) (Sigma-Aldrich), and quickly cut into pieces. The heart pieces were incubated in 5 ml of digesting solution (0.25 mg/ml Liberase TH [Roche] and 10 mM HEPES in balanced salt solution containing calcium and magnesium) for 8 minutes at 37°C with vigorous stirring. The supernatant was then added to 10 ml of ice-cold KHB. Five milliliters of fresh digesting solution was added to the remaining tissue fragments, and the digestion and sampling steps were repeated until all the tissue was dissolved. The collected cells were filtered through 35-μm nylon mesh (BD Falcon) and then used for flow cytometry. Levels of *Myh6* mRNA expression were much lower in the isolated cell populations than in normal whole hearts, indicating that the cell populations obtained using the method described here were enriched in non-myocytes (Supplemental Figure 15). Flow cytometric analysis (Figure 3) showed that the cell populations contained large fractions of fibroblasts and ECs.

Flow cytometric analysis and sorting. Single cells were isolated from adult hearts and incubated with PE-conjugated anti-Thy1 antibody (eBioscience), FITC-conjugated anti-CD31 antibody (BD Biosciences), and allophycocyanin-conjugated CD3e antibody (eBioscience), after which they were analyzed and sorted using a FACSAria II (BD Biosciences) and FlowJo software.

For analysis of β-galactosidase expression and the sorting of $LacZ^+$ cells, a FluoReporter LacZ Flow Cytometry Kit (Molecular Probes, Invitrogen) was used according to the manufacturer's recommendations. Cells were stained with the fluorogenic β-galactosidase substrate fluorescein di-β-D-galactopyranoside (FDG).

Production of medium conditioned by cardiac fibroblasts. Cardiac fibroblasts were grown to subconfluency in 10-cm dishes. The medium was then replaced with fresh serum-free DMEM, and the cells were incubated for additional 48 hours. The medium was then collected as conditioned medium.

siRNA. siRNA for *Klf5* and control siRNA were purchased from Dharmacon. Using Lipofectamine RNAiMax (Invitrogen), the siRNA at a final concentration of 20 nM in 10 ml of culture medium was transfected into mouse cardiac fibroblasts plated in 10-cm culture dishes. siRNA-mediated knockdown of *Klf5* did not affect mRNA expression levels in KLF family members that reportedly function in the cardiovascular system (e.g., *Klf2*, *Klf4*, *Klf10*, *Klf13*, and *Klf15*) (Supplemental Figure 16).

Morphometric studies of cells. Neonatal cardiomyocytes cultured in 3.5-cm dishes were maintained in serum-free DMEM for 24 hours, after which the culture medium was replaced with either fresh serum-free DMEM or medium conditioned by cardiac fibroblasts. To analyze the effects of neutralizing IGF-1, either anti-IGF-1 neutralizing antibody (Millipore) or control IgG (Sigma-Aldrich) was then added, and the cells were cultured for an additional 24 hours. To analyze the effects of growth factors, cells were first cultured for 24 hours in serum-free DMEM. The medium was then replaced with serum-free DMEM containing vehicle, IGF-1 (Wako), or PDGF-A (R&D Systems), and the cells were cultured for an additional 24 hours. The cells were then fixed in 2% paraformaldehyde and permeabilized for 10 minutes with 0.5% Triton X-100 (Sigma-Aldrich) in PBS, after which they were incubated in PBS containing 1% bovine serum albumin for 10 minutes to block nonspecific staining. They were then incubated with anti-sarcomeric α-actinin antibody (Sigma-Aldrich), followed by treatment with an Alexa-conjugated secondary antibody. Cardiomyocyte size was determined by measuring the surface area of sarcomeric α-actinin–positive cells.

Enzyme-linked immunoassay. To analyze secretion of ANP, cardiomyocytes were cultured in the serum-free DMEM for 24 hours and then stimulated with fresh serum-DMEM or medium conditioned by cardiac fibroblasts for 48 hours. The concentration of ANP protein in the culture medium was measured using an enzyme-linked immunoassay kit (Phoenix Pharmaceuticals).

Analysis of expression of alternatively spliced Igf1 mRNA. IGF-1 is controlled by 2 distinct promoters associated with untranslated exons 1 and 2, which generate two types of mRNA, containing either exon 1 (class 1 mRNA) or exon 2 (class 2 mRNA) plus a common block of translated exons (53–55). Expression of the two transcripts is differentially regulated in different tissues and species and during development. We therefore determined which mRNA was the major transcript in mouse heart. The respective abundances of the two transcripts were analyzed using real-time PCR with primer sets that specifically amplified either the class 1 or class 2 mRNA. To calculate absolute numbers of transcripts in a given amount of total RNA, we used external standards containing known numbers of class 1 or 2 cDNA fragments. We found that class 2 transcripts were much more abundant in both cardiac fibroblasts and cardiomyocytes than class 1 transcripts, and also in hearts after LI-TAC (Supplemental Figure 17). We therefore analyzed expression of class 2 mRNA as the major *Igf1* transcript in the heart and cardiac fibroblasts (Figure 6, A–C). *Igf1* class 1 and class 2 cDNA fragments were amplified using a forward primer specific for each leader exon (exon 1, 5′-ATGGGGAAAATCAGCAGTC-3′; exon 2, 5′-CTGCCTGTGTAAACGACCCGG-3′) and a reverse primer (exon 3-4 junction, 5′-GGCTGCTTTTGTAGGCTTCAGTGG-3′) (56).

Igf1 promoter–luciferase constructs. Because the class 2 *Igf1* mRNA is much more abundantly expressed than class 1 mRNA in the heart, we analyzed

the promoter associated with exon 2 (33). A genomic fragment of the 5′-flanking region and a part of exon 2 (-80 to +43 bp) was obtained by PCR using mouse genomic DNA. The promoter fragment was then subcloned into a pGL3 basic luciferase reporter vector (Promega) to generate pGL3-*Igf1*. A mutation within the potential KLF-binding motif was introduced by PCR to generate pGL3-*igf1*mutKLF. NIH-3T3 cells grown to 60%–80% confluence were then transfected with the vectors, after which luciferase activities were measured and normalized to β-galactosidase activity. The *Klf5* expression vector was described previously (57). The *Klf15* expression vector was obtained by inserting the *Klf15* cDNA into pCAGMS (14).

ChIP. ChIP assays were performed as previously described (29, 58). Mouse cardiac fibroblasts were formalin fixed, and then chromatin samples were immunoprecipitated using anti-KLF5 mouse monoclonal antibody (KM3918) or control IgG antibody. PCR was performed with the following region-specific primers: for the mouse *Igf1* KLF5 site within the exon 2–associated promoter, 5′-ACCCAGGCTCAGAGCATACC-3′ and 5′-GGGTCGTTTACACAGCAGGT-3′; for intron 2 (an intronic region +750 bp from the translation initiation site that does not contain KLF-binding motifs; negative control), 5′-CCTTCACCGCTCTCTGAAAC-3′ and 5′-CATCAGGGCTTCATGGTTCT-3′; and for the *Pdgfa* KLF5 site, 5′-ATGTAGCTGCCTGCGTGAG-3′ and 5′-CGACAGGGAGGGGGTTATAG-3′.

Statistics. Data are shown as mean ± SEM. Paired data were evaluated using Student's *t* test. Comparisons between multiple groups were made using 1-way ANOVA followed by a post-hoc Bonferroni test. Survival rates among mice were analyzed using long-rank test. *P* values less than 0.05 were considered statistically significant.

Acknowledgments

We thank N. Yamanaka, Y. Xiao, A. Ono, M. Hayashi, and E. Magoshi for their excellent technical assistance. This study was supported by Grants-in-Aid for Scientific Research (to N. Takeda, I. Manabe, R. Nagai) and a grant for Translational Systems Biology and Medicine Initiative from the Ministry of Education, Culture, Sports, Science and Technology of Japan; a research grant from the National Institute of Biomedical Innovation (to R. Nagai); and a research grant from the Japan Science and Technology Institute (to I. Manabe). P. Snider is supported by NIH T32 HL079995 Training Grant in Vascular Biology and Medicine, and S.J. Conway is partially supported by the Riley Children's Foundation and the NIH.

Received for publication June 24, 2009, and accepted in revised form October 21, 2009.

Address correspondence to: Ryozo Nagai or Ichiro Manabe, Department of Cardiovascular Medicine, University of Tokyo Graduate School of Medicine, 7-3-1 Hongo, Bunkyo, Tokyo 113-8655, Japan. Phone: 81-3-5800-6526; Fax: 81-3-3818-6673; E-mail: nagai-tky@umin.ac.jp (R. Nagai); manabe-tky@umin.ac.jp (I. Manabe).

1. Frey N, Olson EN. Cardiac hypertrophy: the good, the bad, and the ugly. *Annu Rev Physiol.* 2003;65:45–79.
2. Baudino TA, Carver W, Giles W, Borg TK. Cardiac fibroblasts: friend or foe? *Am J Physiol Heart Circ Physiol.* 2006;291(3):H1015–H1026.
3. Manabe I, Shindo T, Nagai R. Gene expression in fibroblasts and fibrosis: involvement in cardiac hypertrophy. *Circ Res.* 2002;91(12):1103–1113.
4. Eghbali M, et al. Collagen chain mRNAs in isolated heart cells from young and adult rats. *J Mol Cell Cardiol.* 1988;20(3):267–276.
5. Zak R. Cell proliferation during cardiac growth. *Am J Cardiol.* 1973;31(2):211–219.
6. Kuwahara K, et al. Involvement of cardiotrophin-1 in cardiac myocyte-nonmyocyte interactions during hypertrophy of rat cardiac myocytes in vitro. *Circulation.* 1999;100(10):1116–1124.
7. Harada M, et al. Significance of ventricular myocytes and nonmyocytes interaction during cardiocyte hypertrophy: evidence for endothelin-1 as a paracrine hypertrophic factor from cardiac nonmyocytes. *Circulation.* 1997;96(10):3737–3744.
8. Sano M, et al. Interleukin-6 family of cytokines mediate angiotensin II-induced cardiac hypertrophy in rodent cardiomyocytes. *J Biol Chem.* 2000;275(38):29717–29723.
9. Oka T, et al. Genetic manipulation of periostin expression reveals a role in cardiac hypertrophy and ventricular remodeling. *Circ Res.* 2007;101(3):313–321.
10. King KL, et al. Phenylephrine, endothelin, prostaglandin F2alpha' and leukemia inhibitory factor induce different cardiac hypertrophy phenotypes in vitro. *Endocrine.* 1998;9(1):45–55.
11. Ieda M, et al. Cardiac fibroblasts regulate myocardial proliferation through beta1 integrin signaling. *Dev Cell.* 2009;16(2):233–244.
12. Thum T, et al. MicroRNA-21 contributes to myocardial disease by stimulating MAP kinase signalling in fibroblasts. *Nature.* 2008;456(7224):980–984.
13. Haldar SM, Ibrahim OA, Jain MK. Kruppel-like Factors (KLFs) in muscle biology. *J Mol Cell Cardiol.* 2007;43(1):1–10.
14. Shindo T, et al. Kruppel-like zinc-finger transcription factor KLF5/BTEB2 is a target for angiotensin II signaling and an essential regulator of cardiovascular remodeling. *Nat Med.* 2002;8(8):856–863.
15. Nagai R, Suzuki T, Aizawa K, Shindo T, Manabe I. Significance of the transcription factor KLF5 in cardiovascular remodeling. *J Thromb Haemost.* 2005;3(8):1569–1576.
16. Forsberg K, Valyi-Nagy I, Heldin CH, Herlyn M, Westermark B. Platelet-derived growth factor (PDGF) in oncogenesis: development of a vascular connective tissue stroma in xenotransplanted human melanoma producing PDGF-BB. *Proc Natl Acad Sci U S A.* 1993;90(2):393–397.
17. Lindahl P, Johansson BR, Leveen P, Betsholtz C. Pericyte loss and microaneurysm formation in PDGF-B-deficient mice. *Science.* 1997;277(5323):242–245.
18. Raines EW. PDGF and cardiovascular disease. *Cytokine Growth Factor Rev.* 2004;15(4):237–254.
19. Andrae J, Gallini R, Betsholtz C. Role of platelet-derived growth factors in physiology and medicine. *Genes Dev.* 2008;22(10):1276–1312.
20. Agah R, et al. Gene recombination in postmitotic cells. Targeted expression of Cre recombinase provokes cardiac-restricted, site-specific rearrangement in adult ventricular muscle in vivo. *J Clin Invest.* 1997;100(1):169–179.
21. Lindsley A, et al. Identification and characterization of a novel Schwann and outflow tract endocardial cushion lineage-restricted periostin enhancer. *Dev Biol.* 2007;307(2):340–355.
22. Joseph NM, et al. The loss of Nf1 transiently promotes self-renewal but not tumorigenesis by neural crest stem cells. *Cancer Cell.* 2008;13(2):129–140.
23. Conway SJ, Molkentin JD. Periostin as a Heterofunctional Regulator of Cardiac Development and Disease. *Current Genomics.* 2008;9(8):548–555.
24. Snider P, et al. Periostin is required for maturation and extracellular matrix stabilization of noncardiomyocyte lineages of the heart. *Circ Res.* 2008;102(7):752–760.
25. Dorn GW, 2nd. Periostin and myocardial repair, regeneration, and recovery. *N Engl J Med.* 2007;357(15):1552–1554.
26. Soriano P. Generalized lacZ expression with the ROSA26 Cre reporter strain. *Nat Genet.* 1999;21(1):70–71.
27. Shioya T. A simple technique for isolating healthy heart cells from mouse models. *J Physiol Sci.* 2007;57(6):327–335.
28. Hudon-David F, Bouzeghrane F, Couture P, Thibault G. Thy-1 expression by cardiac fibroblasts: lack of association with myofibroblast contractile markers. *J Mol Cell Cardiol.* 2007;42(5):991–1000.
29. Oishi Y, et al. SUMOylation of Kruppel-like transcription factor 5 acts as a molecular switch in transcriptional programs of lipid metabolism involving PPAR-delta. *Nat Med.* 2008;14(6):656–666.
30. Serose A, Salmon A, Fiszman MY, Fromes Y. Short-term treatment using insulin-like growth factor-1 (IGF-1) improves life expectancy of the delta-sarcoglycan deficient hamster. *J Gene Med.* 2006;8(8):1048–1055.
31. Abbas A, Grant PJ, Kearney MT. Role of IGF-1 in glucose regulation and cardiovascular disease. *Expert Rev Cardiovasc Ther.* 2008;6(8):1135–1149.
32. McMullen JR. Role of insulin-like growth factor 1 and phosphoinositide 3-kinase in a setting of heart disease. *Clin Exp Pharmacol Physiol.* 2008;35(3):349–354.
33. Wang X, Talamantez JL, Adamo ML. A CACCC box in the proximal exon 2 promoter of the rat insulin-like growth factor I gene is required for basal promoter activity. *Endocrinology.* 1998;139(3):1054–1066.
34. Wang B, et al. The Kruppel-like factor KLF15 inhibits connective tissue growth factor (CTGF) expression in cardiac fibroblasts. *J Mol Cell Cardiol.* 2008;45(2):193–197.
35. Fisch S, et al. Kruppel-like factor 15 is a regulator of cardiomyocyte hypertrophy. *Proc Natl Acad Sci U S A.* 2007;104(17):7074–7079.
36. Ema M, et al. Kruppel-like factor 5 is essential for blastocyst development and the normal self-renewal of mouse ESCs. *Cell Stem Cell.* 2008;3(5):555–567.
37. Parisi S, et al. Klf5 is involved in self-renewal of mouse embryonic stem cells. *J Cell Sci.* 2008;121(Pt 16):2629–2634.
38. Jiang J, et al. A core Klf circuitry regulates self-renewal of embryonic stem cells. *Nat Cell Biol.* 2008;10(3):353–360.
39. Aizawa K, et al. Regulation of platelet-derived growth factor-A chain by Kruppel-like factor 5: new pathway of cooperative activation with nuclear factor-kappaB. *J Biol Chem.* 2004;279(1):70–76.
40. Pietrzkowski Z, Wernicke D, Porcu P, Jameson BA, Baserga R. Inhibition of cellular proliferation by

peptide analogues of insulin-like growth factor 1. *Cancer Res.* 1992;52(23):6447–6451.
41. Sano M, et al. p53-induced inhibition of Hif-1 causes cardiac dysfunction during pressure overload. *Nature.* 2007;446(7134):444–448.
42. Welch S, et al. Cardiac-specific IGF-1 expression attenuates dilated cardiomyopathy in tropomodulin-overexpressing transgenic mice. *Circ Res.* 2002;90(6):641–648.
43. Li B, et al. Insulin-like growth factor-1 attenuates the detrimental impact of nonocclusive coronary artery constriction on the heart. *Circ Res.* 1999;84(9):1007–1019.
44. Kajstura J, et al. IGF-1 overexpression inhibits the development of diabetic cardiomyopathy and angiotensin II-mediated oxidative stress. *Diabetes.* 2001;50(6):1414–1424.
45. Li Q, et al. Overexpression of insulin-like growth factor-1 in mice protects from myocyte death after infarction, attenuating ventricular dilation, wall stress, and cardiac hypertrophy. *J Clin Invest.* 1997;100(8):1991–1999.
46. McMullen JR, et al. The insulin-like growth factor 1 receptor induces physiological heart growth via the phosphoinositide 3-kinase(p110alpha) pathway. *J Biol Chem.* 2004;279(6):4782–4793.
47. Lavallee G, et al. The Kruppel-like transcription factor KLF13 is a novel regulator of heart development. *EMBO J.* 2006;25(21):5201–5213.
48. Subramaniam M, Hawse JR, Johnsen SA, Spelsberg TC. Role of TIEG1 in biological processes and disease states. *J Cell Biochem.* 2007;102(3):539–548.
49. Wakeland E, Morel L, Achey K, Yui M, Longmate J. Speed congenics: a classic technique in the fast lane (relatively speaking). *Immunol Today.* 1997;18(10):472–477.
50. Rockman HA, et al. Segregation of atrial-specific and inducible expression of an atrial natriuretic factor transgene in an in vivo murine model of cardiac hypertrophy. *Proc Natl Acad Sci U S A.* 1991;88(18):8277–8281.
51. Komuro I, et al. Isolation and characterization of two isozymes of myosin heavy chain from canine atrium. *J Biol Chem.* 1986;261(10):4504–4509.
52. Komuro I, et al. Stretching cardiac myocytes stimulates protooncogene expression. *J Biol Chem.* 1990;265(7):3595–3598.
53. Lin WW, Oberbauer AM. Alternative splicing of insulin-like growth factor I mRNA is developmentally regulated in the rat and mouse with preferential exon 2 usage in the mouse. *Growth Horm IGF Res.* 1998;8(3):225–233.
54. Shemer J, Adamo ML, Roberts CT Jr, LeRoith, D. Tissue-specific transcription start site usage in the leader exons of the rat insulin-like growth factor-I gene: evidence for differential regulation in the developing kidney. *Endocrinology.* 1992; 131(6):2793–2799.
55. O'Sullivan DC, Szestak TA, Pell JM. Regulation of IGF-I mRNA by GH: putative functions for class 1 and 2 message. *Am J Physiol Endocrinol Metab.* 2002;283(2):E251–E258.
56. Ohtsuki T, Otsuki M, Murakami Y, Hirata K, Takeuchi S, Takahashi S. Alternative leader-exon usage in mouse IGF-I mRNA variants: class 1 and class 2 IGF-I mRNAs. *Zoolog Sci.* 2007;24(3):241–247.
57. Oishi Y, et al. Kruppel-like transcription factor KLF5 is a key regulator of adipocyte differentiation. *Cell Metab.* 2005;1(1):27–39.
58. Manabe I, Owens GK. CArG elements control smooth muscle subtype-specific expression of smooth muscle myosin in vivo. *J Clin Invest.* 2001;107(7):823–834.

Heart failure causes cholinergic transdifferentiation of cardiac sympathetic nerves via gp130-signaling cytokines in rodents

Hideaki Kanazawa,[1,2] Masaki Ieda,[1,2] Kensuke Kimura,[1] Takahide Arai,[1,2] Haruko Kawaguchi-Manabe,[1] Tomohiro Matsuhashi,[1,2] Jin Endo,[1,2] Motoaki Sano,[1] Takashi Kawakami,[1,2] Tokuhiro Kimura,[3] Toshiaki Monkawa,[2] Matsuhiko Hayashi,[4] Akio Iwanami,[5] Hideyuki Okano,[5] Yasunori Okada,[3] Hatsue Ishibashi-Ueda,[6] Satoshi Ogawa,[2] and Keiichi Fukuda[1]

[1]Department of Regenerative Medicine and Advanced Cardiac Therapeutics, [2]Department of Internal Medicine, [3]Department of Pathology, [4]Department of Apheresis and Dialysis Center, and [5]Department of Physiology, Keio University School of Medicine, Shinjuku-ku, Tokyo, Japan. [6]Department of Pathology, National Cardiovascular Center, Osaka, Japan.

Although several cytokines and neurotrophic factors induce sympathetic neurons to transdifferentiate into cholinergic neurons in vitro, the physiological and pathophysiological roles of this remain unknown. During congestive heart failure (CHF), sympathetic neural tone is upregulated, but there is a paradoxical reduction in norepinephrine synthesis and reuptake in the cardiac sympathetic nervous system (SNS). Here we examined whether cholinergic transdifferentiation can occur in the cardiac SNS in rodent models of CHF and investigated the underlying molecular mechanism(s) using genetically modified mice. We used Dahl salt-sensitive rats to model CHF and found that, upon CHF induction, the cardiac SNS clearly acquired cholinergic characteristics. Of the various cholinergic differentiation factors, leukemia inhibitory factor (LIF) and cardiotrophin-1 were strongly upregulated in the ventricles of rats with CHF. Further, LIF and cardiotrophin-1 secreted from cultured failing rat cardiomyocytes induced cholinergic transdifferentiation in cultured sympathetic neurons, and this process was reversed by siRNAs targeting *Lif* and cardiotrophin-1. Consistent with the data in rats, heart-specific overexpression of LIF in mice caused cholinergic transdifferentiation in the cardiac SNS. Further, SNS-specific targeting of the gene encoding the gp130 subunit of the receptor for LIF and cardiotrophin-1 in mice prevented CHF-induced cholinergic transdifferentiation. Cholinergic transdifferentiation was also observed in the cardiac SNS of autopsied patients with CHF. Thus, CHF causes target-dependent cholinergic transdifferentiation of the cardiac SNS via gp130-signaling cytokines secreted from the failing myocardium.

Introduction

Cardiac function is tightly controlled by the balance between the sympathetic nervous system (SNS) and the parasympathetic nervous system (PNS). The SNS produces norepinephrine (NE) and increases the heart rate, conduction velocity, and myocardial contraction and relaxation, while the PNS produces acetylcholine (Ach) that reduces cardiac performance. In congestive heart failure (CHF), sympathetic neural tone is upregulated, and excess SNS activation leads to pathophysiological effects, such as myocardial damage, decline of cardiac function, and lethal arrhythmia (1, 2), and also causes depletion of cardiac NE content (3). This depletion of NE in CHF has been considered to be the result of excess NE secretion, disturbance of NE reuptake, and loss of noradrenergic nerve terminals (4, 5). However, we recently reported that the attenuation of NE in CHF was caused by downregulation of NE synthesis, concomitant with the reduced NE reuptake (6). However, the molecular mechanisms underlying the reduction in catecholaminergic characteristics of cardiac SNS in CHF remain poorly understood.

Neurotrophic factors that are secreted by the target organ and their target-derived retrograde signals are essential for the development and differentiation of neurons and well as for neuronal diversification and acquisition of neuronal properties (7). Previous studies have established that leukemia inhibitory factor (LIF), a member of the IL-6 cytokine family, can induce cultured sympathetic neurons to switch neurotransmitters, from NE to Ach (8). Fukada purified a cholinergic differentiation factor from cultured rat heart cells that can induce neurotransmitter switching from NE to Ach in cultured sympathetic neurons (9, 10), and Yamamori confirmed that this factor was identical to LIF (11). LIF can induce neurotransmitter switching in vitro and in vivo. Although sweat glands are innervated by catecholaminergic sympathetic nerves at birth, the switch of neurotransmitter from catecholamine to Ach occurs gradually during development (7). Sympathetic neuron-specific gene targeting of gp130, an IL-6 cytokine family receptor, revealed that sympathetic nerves do not undergo cholinergic differentiation in the sweat gland (12). Studies in transgenic mice overexpressing LIF in pancreas show that the catecholaminergic characteristics decline, while the cholinergic characteristics increase (13). These results demonstrate that LIF/gp130 signaling plays an essential role in cholinergic neurotransmitter switching in sympathetic nerves.

Conflict of interest: The authors have declared that no conflict of interest exists.
Citation for this article: *J Clin Invest.* 2010;120(2):408–421. doi:10.1172/JCI39778.

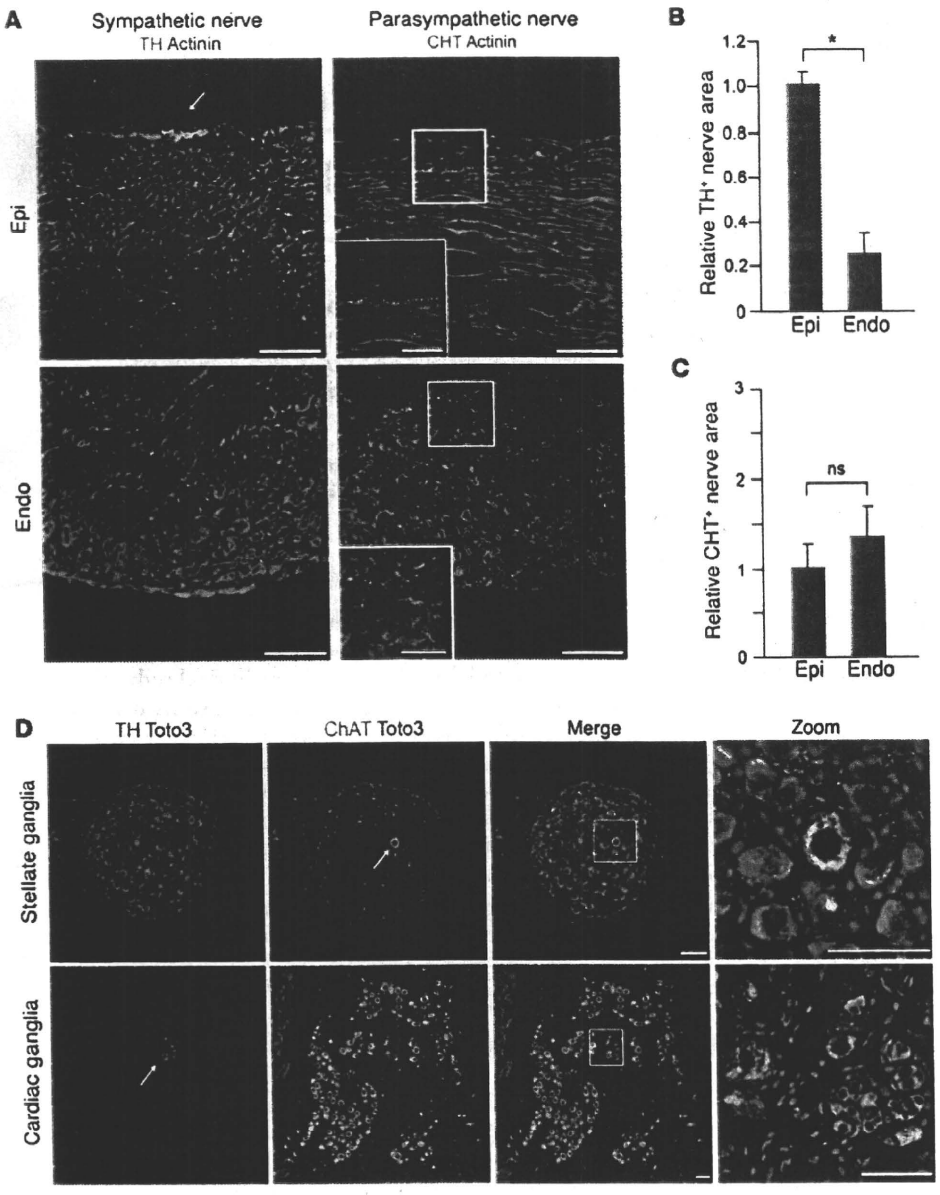

Figure 1
Distribution of sympathetic and parasympathetic nerves in the rat heart. (**A**) Immunofluorescence staining for TH, CHT (green), and α-actinin (red) in the rat LV. TH+ nerves were more abundant in the subepicardial layer (epi) than the subendocardial layer (endo). The arrow indicates sympathetic nerves at the epicardial surface. No CHT+ nerves were observed at the epicardial surface, and CHT+ nerves were more abundant in the subendocardial layer. Higher-magnification views of the boxed regions are shown in the insets. (**B**) Quantitative analysis of TH+ nerve area of LVs ($n = 5$). (**C**) Quantitative analysis of CHT+ nerve area of LVs ($n = 5$). (**D**) Representative immunostaining for TH (red), ChAT (green), and Toto3 (blue) in rat stellate ganglia and cardiac ganglia. A ChAT+ neuron (arrow, top row) was surrounded by TH+ neurons in the stellate ganglia. A few TH+ cells (arrow, bottom row) were observed in cardiac ganglia. Higher-magnification views of the boxed regions in the third column are shown in the fourth column. Representative data are shown in each panel. $^*P < 0.01$. Scale bars: 100 μm (**A**); 50 μm (**A**, insets, and **D**).

CHF leads to upregulation of a range of growth factors and cytokines in the heart (14). LIF and other members of the IL-6 family, which can induce fetal gene expression (so-called rejuvenation) in adult cardiomyocytes, are upregulated during CHF (15, 16). In cardiac SNS in CHF, we also observed strong expression of growth-associated protein 43 (GAP43) and highly polysialylated neural cell adhesion molecule (PSA-NCAM), which are immature neuronal markers expressed specifically in the fetal SNS. This result suggests that cardiac SNS dysfunction is accompanied by neuronal rejuvenation (6). To further understand the precise pathophysiological molecular mechanism, we investigated the relationship between phenotype and paracrine factors in failing myocardium.

In the present study, we show that cardiac SNS in CHF in human hearts and animal models, can cause neurotransmitter switching and transdifferentiation from catecholaminergic into cholinergic neurons, and this process is induced by gp130-mediated signaling via cholinergic differentiation factors released from failing myocardium.

Results

Distribution of sympathetic and parasympathetic nerves in the rat heart. We first defined the sympathetic and parasympathetic innervation of the rat heart. Immunostaining of LVs for tyrosine hydroxylase (TH) and choline transporter (CHT) was performed as a catecholaminergic and cholinergic nerve marker, respectively. TH-immunopositive (TH+) nerves were abundant in LVs, with greater innervation of the subepicardium (Figure 1, A and B) as we previously reported (17). CHT+ nerves were fewer in number than TH+ nerves, and their density was not different between myocardial layers (Figure 1, A and C). The thick and fasciculated nerve fibers at the epicardial surface expressed TH but not CHT (Figure 1A).

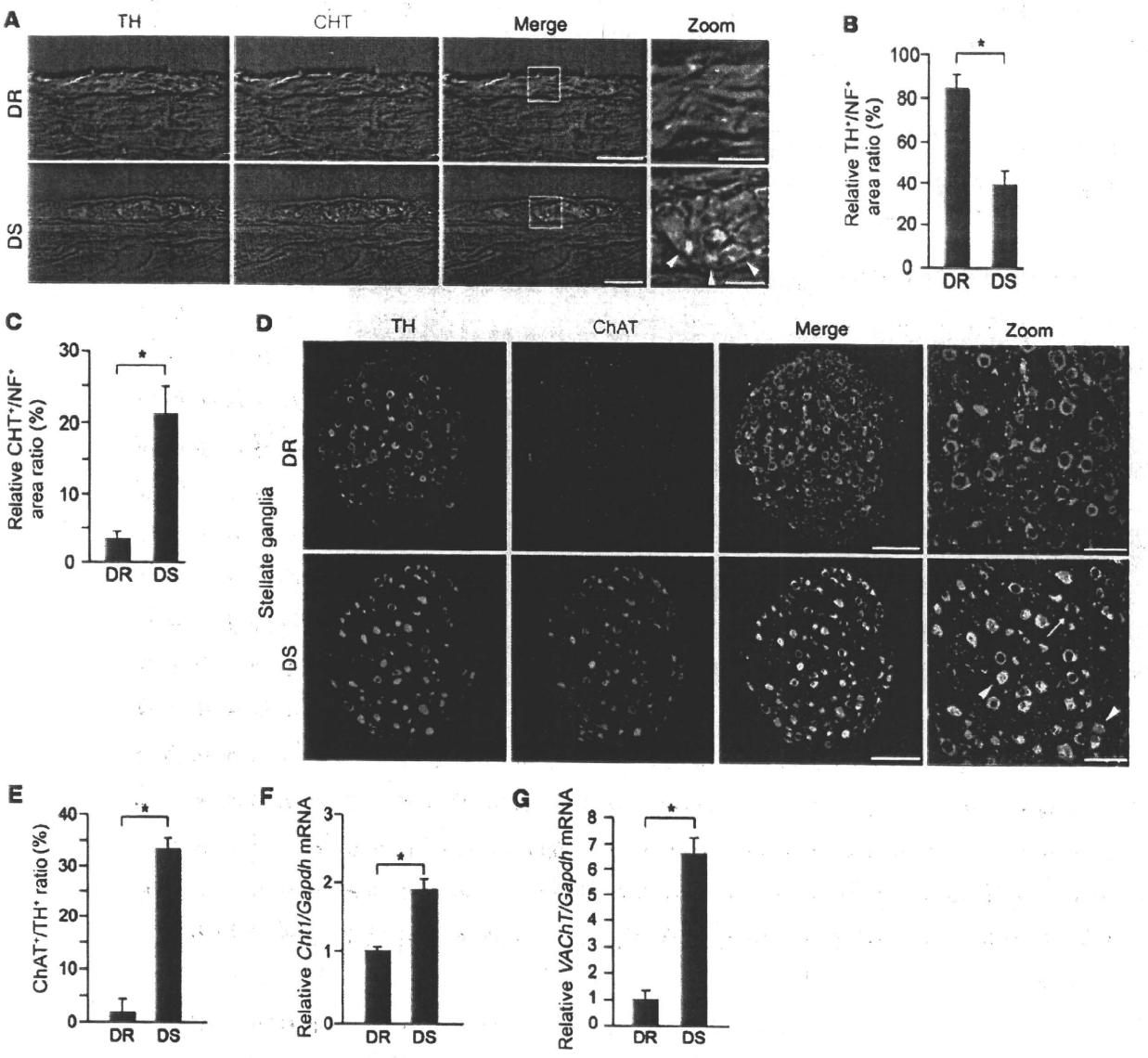

Figure 2

Cardiac nerve fibers and stellate ganglia neurons in DS rat ventricles have both catecholaminergic and cholinergic activity. (**A**) Confocal images of double immunofluorescence staining for TH (red) and CHT (green) in LVs at the epicardium in DR and DS rats. Numbers of CHT+ nerve fibers (arrowheads) were increased, and some nerves coexpressed TH. Higher-magnification views of the boxed regions in the third column are shown in the fourth column. Representative data are shown in each panel. (**B** and **C**) Quantitative analysis of the TH+/NF+ and CHT+/NF+ area ratios in LVs at the epicardium ($n = 5$). (**D**) Double immunostaining with TH (red) and ChAT (green) of the stellate ganglia in DR and DS rats. Note that DS rats had more ChAT+ neurons. Some cells coexpressed TH (arrowheads), some did not (arrow). (**E**) Quantitative analysis of the ChAT+/TH+ ratio in the stellate ganglia ($n = 4$). (**F**) *Cht1* expression in the stellate ganglia of DR and DS rats, determined by qRT-PCR ($n = 4$). (**G**) *VAChT* expression in the stellate ganglia of DR and DS rats, determined by qRT-PCR ($n = 4$). *$P < 0.01$. Scale bars: 20 μm (**A**); 100 μm (**D**); 5 μm (**A**, zoom); 50 μm (**D**, zoom).

In cardiac SNS, preganglionic and postganglionic synapses occur mainly in the stellate ganglia and partially in the upper thoracic ganglia. The vast majority of neurons in the stellate ganglia were TH+, and a few coexpressed choline acetyltransferase (ChAT, a cholinergic nerve marker). In contrast, almost all neurons in the cardiac ganglia were ChAT+, with a few expressing TH (Figure 1D). Thus, catecholaminergic sympathetic innervation is predominant in LVs, and the cardiac SNS and PNS extend from the neurons in stellate and cardiac ganglia, respectively.

Cardiac sympathetic nerve fibers show an increase in cholinergic marker–positive neurons in Dahl salt-sensitive rat ventricles. In Dahl salt-sensitive (DS) rats, high salt intake causes hypertension, cardiac hypertrophy, fibrosis, and DS rats are a common model of CHF. To determine whether cardiac innervation is altered in CHF, we analyzed sympathetic neuronal function in DS rats and the control Dahl salt-resistant (DR) rats (control). DS rats showed elevated blood pressure and heart rate as well as pleural effusion (Supplemental Table 1; supplemental material available online with this article;

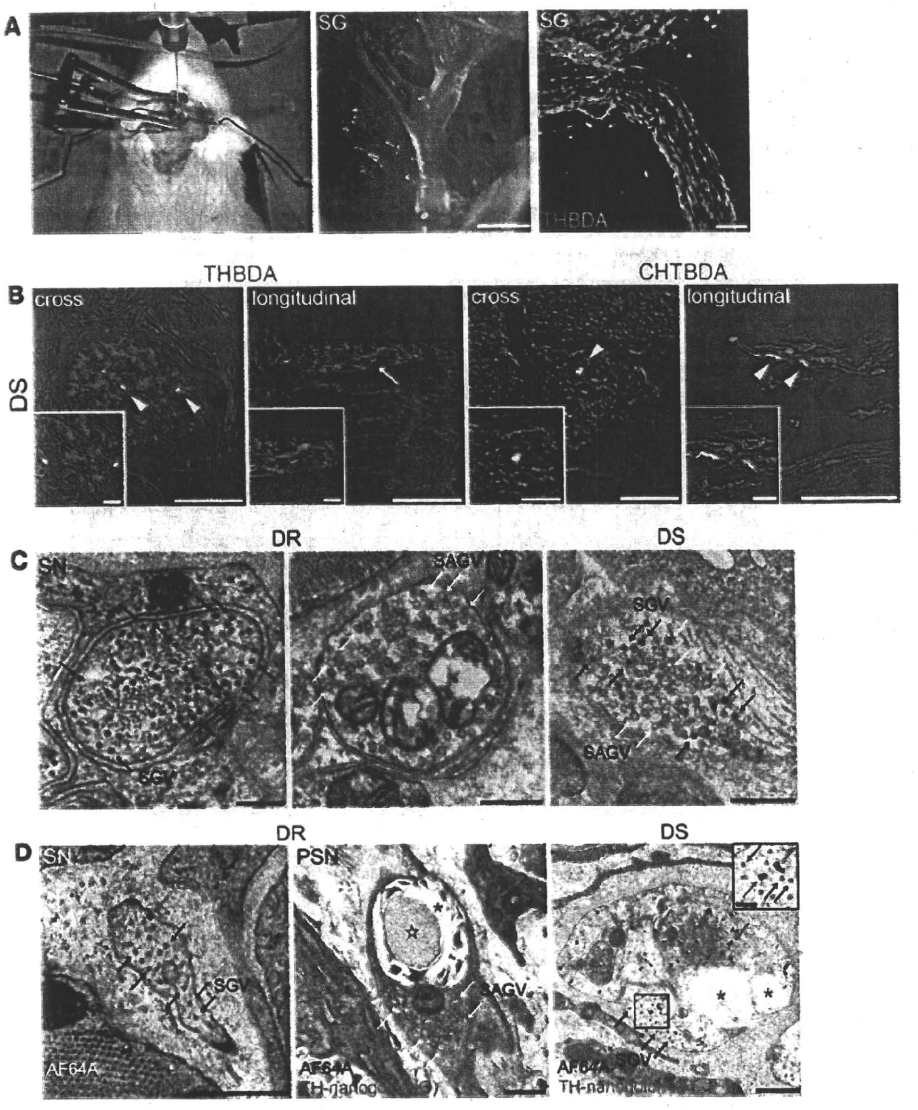

Figure 3

Cardiac sympathetic nerve fibers acquire cholinergic activity in the ventricles of rats with CHF. (**A**) BDA injection into the left stellate ganglion (left panel); a stereomicroscopic image of the stellate ganglion (middle panel); and BDA after injection, visualized as green signals (right panel) are shown. SG, stellate ganglia. (**B**) Epicardial sympathetic nerves in the DS rat LV. BDA (green, arrowheads) was transported to the cardiac sympathetic nerve fascicules. Some fibers coexpressed TH (red, arrowheads), but others did not (arrow). BDA$^+$ nerve fibers (green, arrowheads) coexpressed CHT, indicating CHT$^+$ nerve fibers were derived from sympathetic nerves. Both cross and longitudinal sections are shown. (**C**) Transmission electron micrographs of the nerve endings in DR and DS rat LVs. Black arrows indicate SGVs in sympathetic nerve endings (SN). White arrows indicate SAGVs in parasympathetic nerve endings (PSN). (**D**) Immunoelectron micrographs of nerve endings in DR and DS rat LVs. Rats were injected with AF64A (cholinergic nerve fiber toxin), and the sections were immunostained with TH and silver-enhanced nanogold (NG) particles (red arrows). AF64A induced vacuoles (blue asterisks) and degeneration (blue star). The black arrows indicate SGVs. A higher-magnification view of the boxed region is shown in the inset. Representative data are shown in each panel. Scale bars: 2 mm (**A**, middle panel); 100 μm (**A**, right panel); 50 μm (**B**, left cross section panel and both longitudinal sections); 20 μm (**B**, right cross section panel); 0.5 μm (**C** and **D**); 10 μm (**B**, insets); 0.1 μm (**D**, inset).

doi:10.1172/JCI39778DS1). DS rats demonstrated heart-to-body weight ratios that were 1.7-fold higher than those for DR rats at 15 weeks (Supplemental Figure 1A) and also showed dilated LVs and reduced fractional shortening (Supplemental Table 2). DS rats also showed elevated brain natriuretic peptide (BNP) expression and plasma NE concentrations but significantly lower cardiac NE concentrations, consistent with CHF (Supplemental Figure 1, B–D).

Triple-immunostaining revealed that DS LVs had fewer catecholaminergic nerves (TH$^+$) and more cholinergic nerves (CHT$^+$) than DR LVs (Supplemental Figure 1E). The epicardial sympathetic nerve bundles in DS rats show a marked increase in CHT$^+$ nerves and a marked decrease in TH$^+$ nerves compared with DR rats (Figure 2A and Supplemental Figure 2, A and B). Coexpression of CHT was observed in some TH$^+$ nerves. In DR rats, the majority of these fibers express TH (TH$^+$/neurofilament$^+$ [TH$^+$/NF$^+$] ratio, 84%), and a small proportion coexpress CHT (CHT$^+$/NF$^+$ ratio, 3%). In contrast, DS rats had markedly more CHT$^+$ nerves (CHT$^+$/NF$^+$ ratio, 21%) and fewer TH$^+$ nerves (TH$^+$/NF$^+$ ratio, 39%) than DR rats (Figure 2, B and C). Double immunostaining for calcitonin gene-related peptide (a sensory nerve marker) and NF revealed that the density of sensory nerves in the LV of DS rats was not significantly different from that observed in DR rats (Supplemental Figure 2, C and D). We also performed double immunostaining for NF and dopamine β-hydroxylase (DBH), another marker for sympathetic nerves (Supplemental Figure 3A). We found fewer catecholaminergic (DBH$^+$) nerves in both the LV and stellate ganglia in DS rats than in DR rats. This result is consistent with our findings from TH immunostaining. These changes occur gradually with the progression of cardiac hypertrophy to CHF (Supplemental Figure 4). Taken together, these results show that markers of cholinergic signaling are increased in DS rats, and some cardiac sympathetic nerve fibers contain both catecholaminergic and cholinergic properties in the LV of DS rats.

Stellate ganglia neurons in rats with heart failure have predominantly cholinergic activity. Next, we investigated the expression of specific markers in the stellate ganglia. DR rats showed many TH$^+$ and DBH$^+$ neurons, a few ChAT$^+$ neurons, and many ChAT$^+$ presyn-

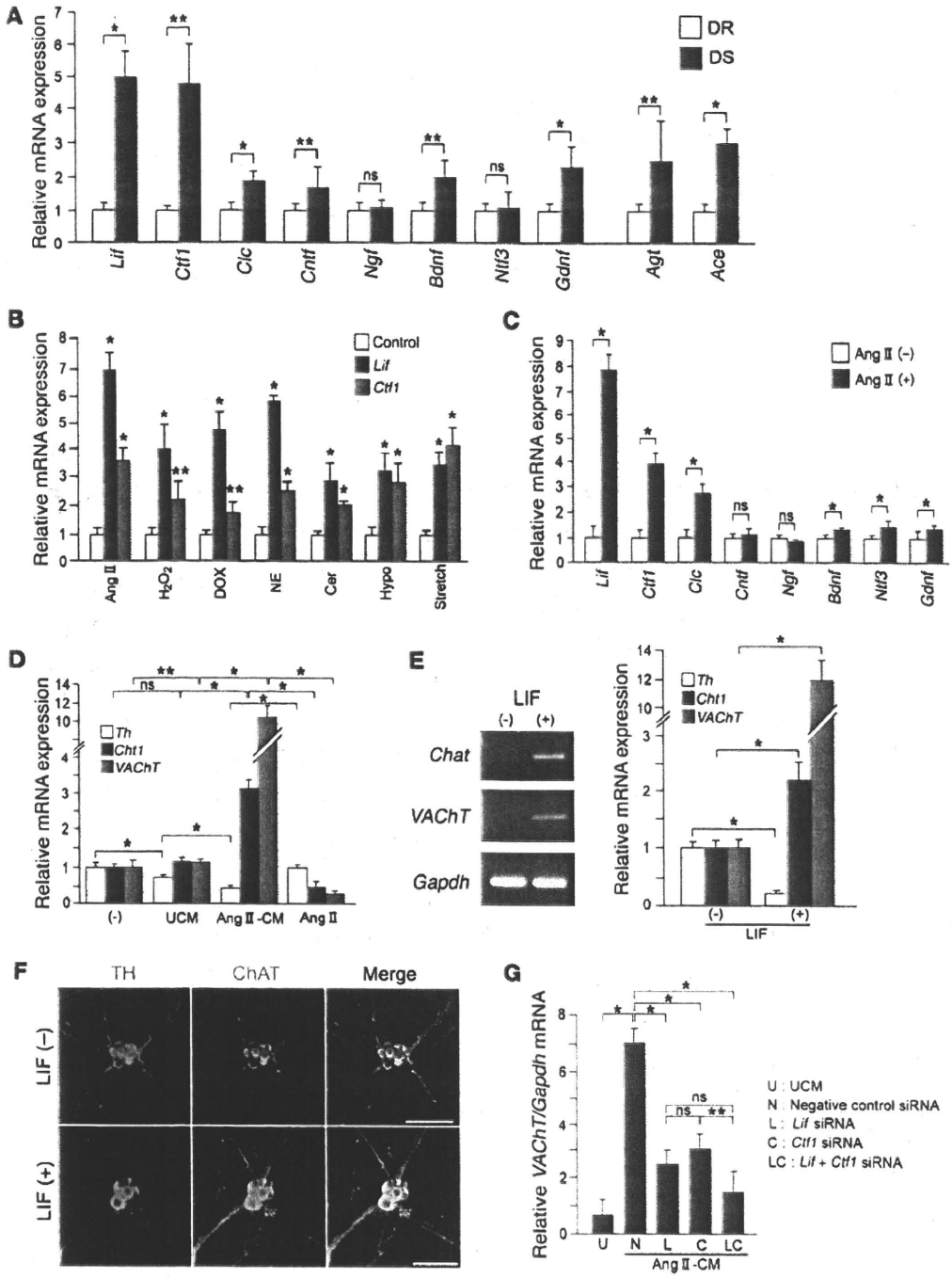

Figure 4

Cardiomyocytes secrete cholinergic differentiation factors that can induce neurotransmitter switching in cultured sympathetic neurons. (**A**) Expression of IL-6 family cytokines (*Lif*, *Ctf1*, cardiotrophin-like cytokine [*Clc*], ciliary neurotrophic factor [*Cntf*]), neurotrophins (nerve growth factor [*Ngf*], brain-derived neurotrophic factor [*Bdnf*], neurotrophin-3 [*Ntf3*]), *Gdnf*, angiotensinogen (*Agt*), and angiotensin-converting enzyme (*Ace*) mRNA in DR and DS rat ventricles was determined by qRT-PCR ($n = 4$–6). (**B**) Primary cultured cardiomyocytes were stimulated with Ang II, H_2O_2, doxorubicin (DOX), NE, ceramide (Cer), hypoxia (5% O_2, Hypo), or 20% mechanical stretch. Expression of *Lif* and *Ctf1* mRNA was investigated using qRT-PCR ($n = 4$). (**C**) Expression of IL-6 family cytokines and neurotrophins in Ang II–CMs were determined by qRT-PCR ($n = 4$). (**D**) Effect of unstimulated and Ang II–CM-conditioned media on the levels of expression of *Th*, *Chat1*, and *VAChT* in cultured sympathetic neurons ($n = 3$). (**E**) Effect of LIF on the levels of expression of *Th*, *Chat1*, and *VAChT* in cultured sympathetic neurons ($n = 3$). RT-PCR analysis of *Chat* and *VAChT* in cultured sympathetic neurons stimulated with LIF. (**F**) Immunocytochemical staining for TH, ChAT, and Toto3 in cultured sympathetic neurons. (**G**) Effect of preincubation of siRNA on the expression of *Lif* and *Ctf1* on *VAChT* in cultured sympathetic neurons. Representative data are shown in each panel. $^*P < 0.01$, $^{**}P < 0.05$ compared with control (**B**); $^*P < 0.01$; $^{**}P < 0.05$ (**A**, **C**–**E**, and **G**). Scale bars: 100 μm.